Conditional and Unconditional Cramér-Rao Bounds for Near-Field Localization in Bistatic MIMO Radar Systems

Liana Khamidullina, *Student Member, IEEE*, Ivan Podkurkov, *Student Member, IEEE*, and Martin Haardt, *Fellow, IEEE*

***Abstract*—The location estimation problem has been attracting a lot of research interest in recent years due to its significance for different areas of signal processing. This paper deals with a bistatic MIMO radar system where the targets are located in the near-field region. In this work, we derive the Cramér-Rao bound (CRB) for bistatic MIMO radar systems using the exact spherical wavefront model to evaluate the performance of target parameter estimation algorithms. The conditional and unconditional CRBs are derived for a system with one and multiple targets. For the one target system, we provide an analytical inversion of the Fisher Information Matrix (FIM) and obtain closed-form analytical non-matrix expressions of the CRB corresponding to the Cartesian and spherical coordinates of the targets. We compare the derived conditional and unconditional CRB with the performance of state-of-the-art localization algorithms and analyse the dependence of the CRB on various system parameters.**

***Index Terms*—Cramér-Rao bound, near-field, radar, source localization, tensor decomposition.**

I. Introduction

DUE to a wide range of applications, parameter estimation is an important field in statistical signal processing. Localization of the radar targets is an important application of parameter estimation algorithms.

There are several assumptions that are commonly made in such source localization problems. Often the wavefronts are assumed to be planar, which corresponds to the far-field assumption [1]. It is only valid if the targets are located relatively far from the antenna array (far-field region). If the targets are closer to the array, several authors use the Fresnel approximation, which employs a second-order Taylor expansion to approximate the wavefronts [2]–[5]. The so-called "Fresnel region" is defined based on the relative distances from the array as compared to the array aperture. The more challenging assumption is the exact spherical wavefront model, which assumes that the wavefronts are spheres centered at the targets/sources [2], [6]–[8]. This assumption closely resembles the physical process under investigation. In this paper, we focus on the latter assumption, i.e., we consider the exact spherical wavefront model of the impinging wavefronts.

Most of the proposed algorithms in the literature are dedicated to sources located in the far-field region or use the Fresnel approximation [9]–[11]. However, in a number of applications, the sources are located in the near-field zone, e.g., health care devices, payment systems, access control, speaker localization [12]–[14]. In those cases, the exact spherical model would allow to increase the estimation accuracy and to estimate the distance to the sources (compared to the far-field assumption). The TeNFiL algorithm, proposed in [8], employs the exact spherical wavefront model and is valid for arrays of arbitrary geometry. This algorithm provides high-resolution target parameter estimates in both two- and three-dimensional (3-D) spaces.

In this paper, we consider target parameter estimation in Bistatic MIMO Radar systems [15]–[19] with two antenna arrays of arbitrary geometry. We obtain deterministic and stochastic Cramér-Rao bounds (CRB) for such systems and compare them with different estimation algorithms.

The CRB is one of the most useful mathematical tools to evaluate the accuracy of different estimation schemes in terms of the mean square error (MSE) [20]. It establishes the minimum achievable variance of an unbiased estimator and allows us to evaluate the performance of different algorithms associated with a specific system model.

In the literature, two types of source signal models are used, the conditional (or deterministic) model and the unconditional (or stochastic) model [21], [22]. In the former case, the signals (or, in our case, reflection coefficients) are assumed to be deterministic but unknown, while in the latter case they are treated as random processes for every realization.

CRBs for different signal models and near-field targets have already been investigated in a number of research works [7], [23]–[31]. In [23], [24], the unconditional (stochastic) CRB (SCRB) is derived in a matrix form (explicit formulas are given only for the elements of the Fisher

Manuscript received November 27, 2020; revised April 9, 2021; accepted May 4, 2021. Date of publication May 21, 2021; date of current version June 11, 2021. The associate editor coordinating the review of this manuscript and approving it for publication was Dr. Bo Tang. This work was supported in part by German Research Foundation (DFG) under Grants HA 2239/14-1 (AdAMMM) and ZH 640/2-1 (AdAMMM), and in part by the Ministry of Education and Science of Russia as part of the fulfillment of obligations under the Agreement number 075-03-2020-051 (topic number fzsu-2020-0020). *(Corresponding author: Liana Khamidullina.)*

Liana Khamidullina and Martin Haardt are with the Communication Research Laboratory, Ilmenau University of Technology, 98693 Ilmenau, Germany (e-mail: liana.khamidullina@tu-ilmenau.de; martin.haardt@tu-ilmenau.de).

Ivan Podkurkov is with the Department of Radioelectronics and Telecommunications Systems, Kazan National Research Technical University named after A. N. Tupolev, Kazan 420111, Russia (e-mail: podkiva@mail.ru).

Digital Object Identifier 10.1109/TSP.2021.3082469

information matrix (FIM)) for a near-field SIMO system using the exact time delay expression. The authors of [25] obtained analytical non-matrix expressions of the conditional and unconditional CRB based on the Fresnel approximation. The conditional (deterministic) CRB (DCRB) using an exact spherical wavefront model is derived in [7]. The authors approximate the obtained formulas for the CRB using the Taylor expansion. All three papers mentioned above ([24], [25], and [7]) consider a uniform linear array (ULA) for the near-field localization of a single source (SIMO case) and estimate the parameters in 2-D space, i.e., only range and angle.

The authors in [32] use the Taylor series expansion of the CRB to obtain an accurate non-matrix closed-form expression of the lower bound of the error for the angle and the range of a near-field source, localized by means of an arbitrary linear array (SIMO case) using the exact wavefront model. They show that the conditional and unconditional CRBs are proportional for an arbitrary parametrization of the steering vector and use the derived CRB to design centro-symmetric linear antenna arrays with improved distance-to-source and angle estimation capabilities.

Recently, the deterministic CRB for a non-uniform linear antenna array with two sources was derived to define the minimum resolvability distance, required to resolve two closely spaced near-field sources [33]. The authors derive the distance resolution limit (DRL) based on Smith's criterion [34] and establish the link between the minimum distance of resolvability and the minimum signal-to-noise ratio (SNR), required to resolve two closely spaced near-field sources. The authors in [35] derive an analytical expression of the angular resolution limit (ARL) for two closely spaced sources. In contrast to our paper, they consider a single array and two point sources in the far-field. Likewise, the authors in [36] and [37] focus on circular periodic estimators, while in this work, we consider a near-field source localization with the additional range parameter. Unlike the aforementioned papers, the authors in [38] consider a bistatic MIMO system with a special circular arc array and derive the CRB for the direction and velocity estimates of a single near-field target.

To the best of our knowledge, non-matrix expressions of the CRB that are obtained via an analytical inversion of the FIM for each estimated parameter are not available for the near-field bistatic MIMO radar system model in 3-D space. Therefore, the main contributions of this paper can be summarized as follows:

- In this paper, we derive the CRB for near-field target localization in 3-D bistatic MIMO radar systems. In particular, we evaluate the conditional and unconditional CRBs for the general near-field system model given in [8] and provide analytical expressions of the conditional and unconditional FIM for such a system with multiple targets.
- We derive closed-form exact expressions of the conditional CRB for bistatic MIMO radar systems with one target. These expressions allow us to reduce the computational cost compared to the matrix-based CRB, especially for a large number of snapshots. Moreover, they provide more insights about the dependence of the bound on different parameters like range, directions, and phases. For example, we show that the CRB of the range increases as the target moves away from the antenna arrays, while the CRB for the angle estimates does not change.
- The CRB derivations are made for the 3-D Cartesian (x, y, and z) and spherical (azimuth ϕ, elevation θ, and range ρ) coordinate systems.
- We use the obtained CRBs to evaluate the performance of state-of-the-art parameter estimation algorithms. Moreover, we use the derived CRBs to analyze the minimum resolvability distance for two closely spaced targets and the impact of the target positions on the estimation accuracy.

This paper is organized as follows. Section II describes the system model used in the paper. In Section III, we present the derivation of the conditional and unconditional CRBs for near-field bistatic MIMO radar systems. The numerical results are provided in Section IV, and the conclusions are drawn in Section V.

Notation: Lower-case and upper-case bold letters denote vectors and matrices, respectively. Upper-case Greek letters denote sets, and boldfaced calligraphic letters denote tensors. The elements of vectors are denoted as follows: $(\boldsymbol{a})_{(i)}$ denotes the i-th element of a vector $\boldsymbol{a}$. The r-mode product between a tensor $\boldsymbol{\mathcal{X}}$ and a matrix $\boldsymbol{A}$ is denoted as $\boldsymbol{\mathcal{X}} \times_r \boldsymbol{A}$ [39]; the Khatri-Rao, Hadamard, and Kronecker products between matrices or vectors are denoted as $\diamond$, $\odot$ and $\otimes$, respectively. The conjugate, transpose, and Hermitian transpose are denoted by $\{\cdot\}^*$, $\{\cdot\}^{\mathrm{T}}$, and $\{\cdot\}^{\mathrm{H}}$, respectively. The $\mathrm{vec}\{\cdot\}$ operator denotes the vectorization operator, and $\Re\{\cdot\}$ denotes the real part. We use $\mathrm{bdiag}\{\cdot\}$ for the operation of creating a block-diagonal matrix by aligning the input matrices on its diagonal. To facilitate the notation, in the following, we assume that the symbols x, y and z will always refer to the Cartesian coordinates of the targets or antennas. Furthermore, the symbols ρ, ϕ, and θ will always denote the distance, azimuth, and elevation of the targets, respectively.

II. System Model

We consider a bistatic MIMO radar system with M_T transmit and M_R receive antennas. Each transmitter emits temporally orthogonal signals which impinge on H point targets, and their reflections are intercepted by the receive array. The targets are assumed to be in the near-field zone of both arrays, such that the wavefronts of the impinging and reflecting waves can be considered as spherical. Consequently, the received signal for N snapshots can be expressed in a tensor form [8]

$$\boldsymbol{\mathcal{Y}} = \boldsymbol{\mathcal{I}}_{3,H} \times_1 \boldsymbol{A} \times_2 \boldsymbol{B} \times_3 \boldsymbol{D} + \boldsymbol{\mathcal{Z}} \in \mathbb{C}^{M_T \times M_R \times N}, \quad (1)$$

or in a matrix form [6]

$$\boldsymbol{Y} = [\boldsymbol{\mathcal{Y}}]^{\mathrm{T}}_{(3)} = (\boldsymbol{A} \diamond \boldsymbol{B})\boldsymbol{D}^{\mathrm{T}} + [\boldsymbol{\mathcal{Z}}]^{\mathrm{T}}_{(3)} \in \mathbb{C}^{M_T M_R \times N}, \quad (2)$$

where $\boldsymbol{\mathcal{Y}}$ contains the received data after matched filtering (assuming unit transmit power), $[\boldsymbol{\mathcal{Y}}]_{(3)}$ denotes the 3-mode unfolding of the tensor $\boldsymbol{\mathcal{Y}}$, which is obtained by stacking its 3-mode vectors into a matrix in reverse-cyclical order [39]. The tensor $\boldsymbol{\mathcal{Z}}$ contains independently and identically distributed (i.i.d.) zero mean spatially and temporally white additive noise with variance σ^2, the matrix $\boldsymbol{D} = \begin{bmatrix} \boldsymbol{d}_1 & \boldsymbol{d}_2 & \dots & \boldsymbol{d}_H \end{bmatrix} \in \mathbb{C}^{N \times H}$

contains the complex reflection coefficients for each target in each snapshot, and $\boldsymbol{\mathcal{I}}_{3,H}$ is a tree-dimensional identity tensor of size $H \times H \times H$. The elements of $\boldsymbol{D}$ are defined as

$$(\boldsymbol{d}_h)_{(k)} = \alpha_h(k) e^{j\psi_h(k)}, k = 1, \ldots, N, \tag{3}$$

where $\alpha_h(k)$ and $\psi_h(k)$ are the amplitudes and phases of the h-th target at the snapshot k, respectively. The matrices $\boldsymbol{A} = \begin{bmatrix} \boldsymbol{a}_1 & \boldsymbol{a}_2 & \ldots & \boldsymbol{a}_H \end{bmatrix}$ and $\boldsymbol{B} = \begin{bmatrix} \boldsymbol{b}_1 & \boldsymbol{b}_2 & \ldots & \boldsymbol{b}_H \end{bmatrix}$ represent the complex transmit and receive array steering matrices, respectively, composed of the array steering vectors for each target. The m-th element of the vector $\boldsymbol{a}$ is defined as

$$(\boldsymbol{a}_h)_{(m)} = e^{-j\delta_{m,h}^{(T)}}, \tag{4}$$

and the n-th element of the vector $\boldsymbol{b}$ is equal to

$$(\boldsymbol{b}_h)_{(n)} = e^{-j\delta_{n,h}^{(R)}}, \tag{5}$$

where $\delta_{m,h}^{(T)}$ is the path difference between the reference transmit antenna and the m-th antenna in the transmit array as provided in (6) on the bottom of this page, and $\delta_{n,h}^{(R)}$ is the path difference between the reference receive antenna and the n-th antenna in the receive array as provided in (7) on the bottom of this page. The path differences are defined based on the exact spherical wavefront model.

We consider target parameters estimation in the full $3-$D space. Therefore, the location parameters to be estimated are the azimuth ϕ, elevation θ, and range ρ for the spherical coordinates system or x, y, and z in case of the Cartesian coordinates.

The antenna arrays are assumed to be of an arbitrary geometry. Each antenna in the array is defined by the set of Cartesian coordinates with respect to the origin of the local system of coordinates that is located either at the transmit or at the receive reference antenna as depicted in Fig. 1. The m-th transmit and the n-th receive antennas of the arrays have Cartesian coordinates $\{x_{T,m}, y_{T,m}, z_{T,m}\}, \forall m \in \{1, \ldots, M_T\}$ and $\{x_{R,n}, y_{R,n}, z_{R,n}\}, \forall n \in \{1, \ldots, M_R\}$, respectively. The coordinates $\{x_R, y_R, z_R\}$ define the position of the reference receive antenna with respect to the reference antenna of the transmit array; and the coordinates of the transmit reference antenna with respect to receive array are defined as $\{x_T, y_T, z_T\}$.

It is assumed that the locations of the transmit and the receive arrays are known, and two position estimates can be obtained for each target (they might not coincide). Therefore, each target in the scenario is characterized by a set of six parameters: $\boldsymbol{\Theta}_h^{(s)} = \{\rho_{T,h}, \phi_{T,h}, \theta_{T,h}, \rho_{R,h}, \phi_{R,h}, \theta_{R,h}\}, \forall h \in \{1, \ldots, H\}$,

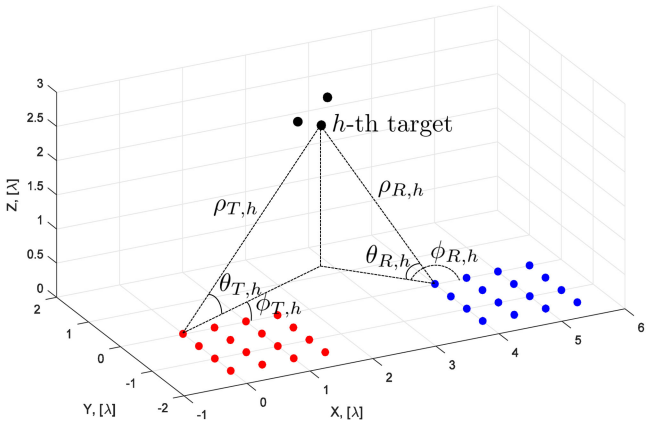

Fig. 1. 3-D System Model. The transmit and receive arrays are depicted using red and blue dots, respectively. The first antennas of the arrays are chosen as reference antennas. The black dots denote radar targets. The figure also shows the six parameters of one of the targets.

where $\rho_{T,h}$ is the distance from the reference transmit antenna to the h-th target, $\rho_{R,h}$ is the distance from reference receive antenna to the h-th target, $\phi_{T,h}$, $\phi_{R,h}$ are the azimuths defined with respect to the reference transmit and receive antennas, respectively, $\theta_{T,h}, \theta_{R,h}$ are the elevation angles also defined with respect to the reference transmit and receive antennas. We also introduce a set of Cartesian coordinates for the h-th target as $\boldsymbol{\Theta}_h^{(c)} = \{x_{T,h}, y_{T,h}, z_{T,h}, x_{R,h}, y_{R,h}, z_{R,h}\}, \forall h \in \{1, \ldots, H\}$, also defined with respect to reference transmit and reference receive antennas.

An example scenario of the system with two uniform rectangular arrays (URAs) is depicted in Fig. 1.

Note that we compute the CRBs separately for the estimates obtained from the transmit and the receive sides: in the equations (6) and (7) for the path differences, all the coordinates are defined either with respect to the transmit reference antenna or the receive reference antenna, depending on the calculated CRB. Thus, for simplicity, we have skipped the T and R indices in the notation of target coordinates $\{x_h, y_h, z_h\}$.

III. Cramér-Rao Bound Derivation

In this section, we provide the main steps of the CRB derivation for the conditional and unconditional signal models with respect to the location parameters of the near-field targets.

Let us consider the real valued parameter vector $\boldsymbol{\xi}$ and its unbiased estimator $\hat{\boldsymbol{\xi}}$. The covariance matrix of $\hat{\boldsymbol{\xi}}$ is $\boldsymbol{R} = \mathbb{E}\{(\hat{\boldsymbol{\xi}} -$

$$\delta_{m,h}^{(T)} = \frac{2\pi}{\lambda}\left(\sqrt{(x_h - x_{T,m})^2 + (y_h - y_{T,m})^2 + (z_h - z_{T,m})^2} - \sqrt{(x_h - x_{T,1})^2 + (y_h - y_{T,1})^2 + (z_h - z_{T,1})^2}\right) \tag{6}$$

$$\delta_{n,h}^{(R)} = \frac{2\pi}{\lambda}\left(\sqrt{(x_h - x_{R,n})^2 + (y_h - y_{R,n})^2 + (z_h - z_{R,n})^2} - \sqrt{(x_h - x_{R,1})^2 + (y_h - y_{R,1})^2 + (z_h - z_{R,1})^2}\right) \tag{7}$$

$$\frac{\partial \delta_{m,h}^{(T)}}{\partial x_h} = \frac{2\pi}{\lambda}\left(\frac{x_h - x_{T,m}}{\sqrt{(x_h - x_{T,m})^2 + (y_h - y_{T,m})^2 + (z_h - z_{T,m})^2}} - \frac{x_h}{x_h^2 + y_h^2 + z_h^2}\right) \tag{8}$$

$$\frac{\partial \delta_{n,h}^{(R)}}{\partial x_h} = \frac{2\pi}{\lambda}\left(\frac{x_h - x_{R,n}}{\sqrt{(x_h - x_{R,n})^2 + (y_h - y_{R,n})^2 + (z_h - z_{R,n})^2}} - \frac{x_h - x_{R,1}}{(x_h - x_{R,1})^2 + (x_h - x_{R,1})^2 + (x_h - x_{R,1})^2}\right) \tag{9}$$

$\boldsymbol{\xi})(\hat{\boldsymbol{\xi}}-\boldsymbol{\xi})^{\mathrm{T}}\}$, and the ith diagonal element of the covariance matrix is the mean-squared error of the estimator $\hat{\xi}_i, i=1,2,\ldots,P$, where P is the size of the parameter vector. Since the estimator $\hat{\boldsymbol{\xi}}$ is unbiased, the mean-squared error is equal to the variance of the estimator, and the lower bound of the variance of the ith parameter satisfies

$$\mathrm{MSE}\{\hat{\xi}_i\} \geq [\mathbf{CRB}(\boldsymbol{\xi})]_{ii}\,, \tag{10}$$

where $[\mathbf{CRB}(\boldsymbol{\xi})]$ is the inverse of the Fisher Information Matrix:

$$[\mathbf{CRB}(\boldsymbol{\xi})] = [\mathbf{FIM}(\boldsymbol{\xi})]^{-1}. \tag{11}$$

Each element of the FIM is defined as [40]

$$[\mathbf{FIM}(\boldsymbol{\xi})]_{ij} = -\mathbb{E}\left[\frac{\partial^2 l(\boldsymbol{\xi})}{\partial\xi_i\partial\xi_j}\right] = \mathbb{E}\left[\frac{\partial l(\boldsymbol{\xi})}{\partial\xi_i}\frac{\partial l(\boldsymbol{\xi})}{\partial\xi_j}\right], \tag{12}$$

where $i=1,2,\ldots,P, j=1,2,\ldots,P, l(\boldsymbol{\xi})$ is the log-likelihood function: $l(\boldsymbol{\xi})=\ln f_{\xi}(\boldsymbol{y})$, and $f_{\xi}(\boldsymbol{y})$ is the probability density function (PDF) parametrized by the parameter $\boldsymbol{\xi}$. Since we consider a Gaussian distribution model, the PDF of the observed data is given by [41]

$$f_{\xi}(\boldsymbol{y}) = \frac{1}{\sqrt{\pi^{M_T M_R N}\det(\boldsymbol{R})}}\exp\left(-(\boldsymbol{y}-\boldsymbol{\mu})^H\boldsymbol{R}^{-1}(\boldsymbol{y}-\boldsymbol{\mu})\right), \tag{13}$$

where $\boldsymbol{y}=\mathrm{vec}\{\boldsymbol{\mathcal{Y}}\}$ is a vectorized received data tensor with mean $\boldsymbol{\mu}$ and covariance matrix $\boldsymbol{R}$, which depends on the chosen deterministic or stochastic assumption. The FIM matrix corresponding to the Gaussian distribution is given by [41]

$$[\mathbf{FIM}(\boldsymbol{\xi})]_{ij} = \mathrm{tr}\left[\boldsymbol{R}^{-1}\frac{\partial\boldsymbol{R}}{\partial\xi_i}\boldsymbol{R}^{-1}\frac{\partial\boldsymbol{R}}{\partial\xi_j}\right] + 2\Re\left[\frac{\partial\boldsymbol{\mu}^H}{\partial\xi_i}\boldsymbol{R}^{-1}\frac{\partial\boldsymbol{\mu}}{\partial\xi_j}\right]. \tag{14}$$

As it can be seen from (14), the FIM depends on the parameter vector $\boldsymbol{\xi}$ and, consequently, on the chosen source model. In the following, we will consider two models, depending on the assumption made on the matrix of complex reflection coefficients $\boldsymbol{D}$:

(1) *conditional* ("deterministic") model, in which the signals are assumed to be deterministic, but unknown, and the same in all realizations, and
(2) *unconditional* ("stochastic") model, which assumes the reflection coefficients (in general, the signals) to be a realization of a Zero-Mean Circularly Symmetric Complex Gaussian (ZMCSCG) process.

We denote the conditional (deterministic) CRB and the conditional FIM (CFIM) with respect to the parameter vector $(\boldsymbol{\xi})$ as $\mathbf{DCRB}(\boldsymbol{\xi})$ and $\mathbf{CFIM}(\boldsymbol{\xi})$, respectively. The unconditional (stochastic) CRB is denoted as $\mathbf{SCRB}(\boldsymbol{\xi})$, and the unconditional FIM (UFIM) as $\mathbf{UFIM}(\boldsymbol{\xi})$. In the following, we will provide closed-form expressions of the $\mathbf{CFIM}(\boldsymbol{\xi})$ and $\mathbf{UFIM}(\boldsymbol{\xi})$ for the general 3-D scenario with multiple targets. For the conditional one target scenario, we will perform an analytical inversion of the FIM and provide closed-form expressions of the $\mathbf{DCRB}(\boldsymbol{\xi})$. In the next sections, we will first derive the CRBs for Cartesian coordinates of the targets and then obtain the CRBs for the spherical coordinates of the targets.

A. Conditional Cramér-Rao Bound

1) Multiple Target Case: First, we focus on the first assumption, that $\boldsymbol{D}$ is deterministic.

For the subsequent calculations, we rewrite the data tensor $\boldsymbol{\mathcal{Y}}$ in a vector form:

$$\boldsymbol{y} = \mathrm{vec}(\boldsymbol{\mathcal{Y}}) = (\boldsymbol{D}\diamond\boldsymbol{B}\diamond\boldsymbol{A})\mathbf{1}_H + \boldsymbol{z}, \tag{15}$$

where $\boldsymbol{y}\in\mathbb{C}^{M_T M_R N\times 1}$, $\diamond$ denotes the Khatri-Rao (column-wise Kronecker) product, $\mathbf{1}_H$ is a vector of ones of size H, and $\boldsymbol{A}$, $\boldsymbol{B}$, and $\boldsymbol{D}$ are the array steering matrices of the transmit and receive arrays, and the matrix of complex reflection coefficients, respectively, which are defined in (1). The noise term, $\boldsymbol{z}=\mathrm{vec}\{\boldsymbol{\mathcal{Z}}\}\in\mathbb{C}^{M_T M_R N\times 1}$ is assumed to be a realization of the ZMCSCG process with a variance σ^2 and covariance matrix

$$\boldsymbol{R} = \sigma^2\boldsymbol{I}_{M_T M_R N}. \tag{16}$$

Due to the deterministic signal model and the ZMCSCG noise, the received signal $\boldsymbol{y}$ is a complex Gaussian random process with mean $\boldsymbol{\mu}=(\boldsymbol{D}\diamond\boldsymbol{B}\diamond\boldsymbol{A})\mathbf{1}_H\in\mathbb{C}^{M_T M_R N\times 1}$ and covariance matrix $\boldsymbol{R}$. The equation (14) for the FIM becomes [41]

$$[\mathbf{CFIM}(\boldsymbol{\xi})]_{ij} = \frac{M_T M_R N}{\sigma^4}\frac{\partial\sigma^2}{\partial\xi_i}\frac{\partial\sigma^2}{\partial\xi_j} + \frac{2}{\sigma^2}\Re\left[\frac{\partial\boldsymbol{\mu}^H}{\partial\xi_i}\frac{\partial\boldsymbol{\mu}}{\partial\xi_j}\right]. \tag{17}$$

For the considered deterministic model, the unknown parameter vector is

$$\boldsymbol{\xi} = [\boldsymbol{p}, \angle\{\mathrm{vec}(\boldsymbol{D})\}^{\mathrm{T}}, |\mathrm{vec}(\boldsymbol{D})|^{\mathrm{T}}, \sigma^2]^{\mathrm{T}}\in\mathbb{R}^{P\times 1}, \tag{18}$$

where $\boldsymbol{p}=[x_1,y_1,z_1,\ldots,x_H,y_H,z_H]^{\mathrm{T}}$ is the vector of target location coordinates, $\angle\{\cdot\}$ and $|\cdot|$ denote the phases and the amplitudes in $\mathrm{vec}(\boldsymbol{D})$, and σ^2 is the noise variance. Note that the parameter vector contains the target coordinates which are defined either with respect to the transmit or to the receive reference antenna. To calculate the CRB for the estimates, obtained from the transmit side, we define the target coordinates $\{x_h,y_h,z_h\}$ and all the antenna coordinates with respect to the transmit array reference antenna, and vice versa for the receive side CRB. For example, equations (8) and (9) on the bottom of the previous page show the derivatives of the path differences with respect to x_h, if the origin of the system of coordinates is at the transmit reference antenna.

Since the parameter vector contains the 3-D Cartesian coordinates of the targets, its size is equal to $P=(3+2N)H+1$, where H is the number of targets, and N is the number of snapshots.

Fisher Information Matrix (FIM). Let us construct the FIM for the multiple targets scenario, using equation (17) and the parameter vector $\boldsymbol{\xi}=[\boldsymbol{p}_1,\ldots,\boldsymbol{p}_H,\boldsymbol{\psi}_1^T,\ldots,\boldsymbol{\psi}_H^T,\boldsymbol{\alpha}_1^T,\ldots,\boldsymbol{\alpha}_H^T,\sigma^2]^{\mathrm{T}}\in\mathbb{R}^{P\times 1}$, where, according to equation (3), $\boldsymbol{\psi}_h^T$ and $\boldsymbol{\alpha}_h^T$ are vectors of the phases and the amplitudes of the complex reflections coefficients at each snapshot, respectively.

As it can be seen from (17), the noise variance σ^2 is decoupled from the other parameters. Thus, for notational simplicity and without loss of generality, we can drop it from the parameter vector $\boldsymbol{\xi}$ and compute the FIM without taking σ^2 into account.

Consequently, the structure of the CFIM is as follows

$$\mathbf{CFIM}(\boldsymbol{\xi}) = \left[\begin{array}{c|cc} \boldsymbol{F}_{\boldsymbol{pp}} & \boldsymbol{F}_{\boldsymbol{p\psi}} & \boldsymbol{F}_{\boldsymbol{p\alpha}} \\ \hline \boldsymbol{F}_{\boldsymbol{\psi p}} & \boldsymbol{F}_{\boldsymbol{\psi\psi}} & \boldsymbol{F}_{\boldsymbol{\psi\alpha}} \\ \boldsymbol{F}_{\boldsymbol{\alpha p}} & \boldsymbol{F}_{\boldsymbol{\alpha\psi}} & \boldsymbol{F}_{\boldsymbol{\alpha\alpha}} \end{array}\right], \tag{19}$$

where the subscripts in the notation of the submatrices denote the corresponding elements of the parameter vector $\boldsymbol{\xi}$, with respect to which partial derivatives are computed in (17).

Such a structure of the FIM has already been considered in [33] for the special case of two sources. There the derived CRB is used to investigate the resolution limit of two closely spaced sources. The authors of the paper consider a single uniform linear antenna array and obtain the CRB for the range and for the azimuth, considering the Fresnel approximation. In our case, we extend it to the bistatic MIMO radar scenario with multiple targets and 3-D location parameters estimation using the exact spherical wavefront model. Each block matrix of the FIM in (19) is composed of submatrices with the elements that are computed according to (17). For more details on the derivation of the elements of the CFIM in (19), we refer the reader to Appendix A.

2) One Target Case: As a special case, let us consider a system scenario with a single target, i.e., $H = 1$. In this case, $\boldsymbol{A}$, $\boldsymbol{B}$, and $\boldsymbol{D}$ in equation (15) turn into column vectors, and the received data can be written as

$$\boldsymbol{y} = \mathrm{vec}(\boldsymbol{\mathcal{Y}}) = \underbrace{(\boldsymbol{d} \diamond \boldsymbol{b} \diamond \boldsymbol{a})}_{\boldsymbol{\mu}} + \boldsymbol{z}, \tag{20}$$

where $\boldsymbol{y} \in \mathbb{C}^{M_T M_R N \times 1}$. In this case, the unknown, but deterministic parameter vector $\boldsymbol{\xi}$ contains the parameters corresponding to one target:

$$\boldsymbol{\xi} = [x, y, z, \boldsymbol{\psi}^{\mathrm{T}}, \boldsymbol{\alpha}^{\mathrm{T}}, \sigma^2]^{\mathrm{T}} \in \mathbb{R}^{(2N+4)}, \tag{21}$$

where x, y, and z are the Cartesian coordinates of a single target, and $\boldsymbol{\psi} = [\psi(1), \ldots, \psi(N)]^{\mathrm{T}}$ and $\boldsymbol{\alpha} = [\alpha(1), \ldots, \alpha(N)]^{\mathrm{T}}$ are the phases and the amplitudes of the reflection coefficients at each snapshot, respectively.

Fisher Information Matrix. As defined in (11), the CRB is equal to the inverse of the FIM. Let us first define the conditional FIM, and then perform its analytical inversion to obtain the non-matrix expressions of the DCRB for the location parameters of the one near-field target.

Based on the data model presented in (20), using equation (17) and the parameter vector $\boldsymbol{\xi}$, we construct the conditional FIM, which has a block-diagonal structure:

$$\mathbf{CFIM}(\boldsymbol{\xi}) = \mathrm{bdiag}(\boldsymbol{Q}, \boldsymbol{J}) \in \mathbb{R}^{(2N+4)\times(2N+4)}, \tag{22}$$

where

$$\boldsymbol{Q} = \left[\begin{array}{ccc|c} f_{xx} & f_{xy} & f_{xz} & \boldsymbol{f}_{x\boldsymbol{\psi}}^{\mathrm{T}} \\ f_{yx} & f_{yy} & f_{yz} & \boldsymbol{f}_{y\boldsymbol{\psi}}^{\mathrm{T}} \\ f_{zx} & f_{zy} & f_{zz} & \boldsymbol{f}_{z\boldsymbol{\psi}}^{\mathrm{T}} \\ \hline \boldsymbol{f}_{\boldsymbol{\psi}x} & \boldsymbol{f}_{\boldsymbol{\psi}y} & \boldsymbol{f}_{\boldsymbol{\psi}z} & \boldsymbol{F}_{\boldsymbol{\psi\psi}} \end{array}\right] = \underbrace{\left[\begin{array}{cc} \boldsymbol{F}_{\boldsymbol{pp}} & \boldsymbol{F}_{\boldsymbol{p\psi}} \\ \boldsymbol{F}_{\boldsymbol{\psi p}} & \boldsymbol{F}_{\boldsymbol{\psi\psi}} \end{array}\right]}_{\in \mathbb{R}^{(N+3)\times(N+3)}}, \tag{23}$$

$$\boldsymbol{J} = \mathrm{bdiag}\left(\underbrace{\frac{2M_T M_R}{\sigma^2}\boldsymbol{I}_N}_{\boldsymbol{F}_{\boldsymbol{\alpha\alpha}}}, \frac{M_T M_R N}{\sigma^4}\right), \tag{24}$$

and bdiag denotes a block-diagonal operator.

The subscripts in (23) denote the corresponding element of the parameter vector, with respect to which the partial derivatives are computed in (17).

The structure of the FIM is explained by the fact that the noise variance σ^2 is decoupled from the other parameters, as it can be seen from (17), and the other zero terms appear due to the time diversity of the signals and due to the fact that the real part operator $\Re$ in (17) is applied on pure imaginary values (see Appendix B for the detailed derivations of the elements of the matrix $\boldsymbol{Q}$ in (23)).

$$\begin{aligned} &\mathrm{DCRB}(x) \\ &= \frac{1}{\det(\boldsymbol{S})}\left(\left(f_{yy} - \frac{2\|\boldsymbol{\alpha}\|^2}{M_T M_R \sigma^2}u_y^2\right)\left(f_{zz} - \frac{2\|\boldsymbol{\alpha}\|^2}{M_T M_R \sigma^2}u_z^2\right)\right. \\ &\quad \left. - \left(f_{yz} - \frac{2\|\boldsymbol{\alpha}\|^2}{M_T M_R \sigma^2}u_y u_z\right)^2\right) \end{aligned} \tag{25}$$

$$\begin{aligned} &\mathrm{DCRB}(y) = \\ &\frac{1}{\det(\boldsymbol{S})}\left(\left(f_{xx} - \frac{2\|\boldsymbol{\alpha}\|^2}{M_T M_R \sigma^2}u_x^2\right)\left(f_{zz} - \frac{2\|\boldsymbol{\alpha}\|^2}{M_T M_R \sigma^2}u_z^2\right)\right. \\ &\quad \left. - \left(f_{xz} - \frac{2\|\boldsymbol{\alpha}\|^2}{M_T M_R \sigma^2}u_x u_z\right)^2\right) \end{aligned} \tag{26}$$

$$\begin{aligned} &\mathrm{DCRB}(z) \\ &= \frac{1}{\det(\boldsymbol{S})}\left(\left(f_{xx} - \frac{2\|\boldsymbol{\alpha}\|^2}{M_T M_R \sigma^2}u_x^2\right)\left(f_{yy} - \frac{2\|\boldsymbol{\alpha}\|^2}{M_T M_R \sigma^2}u_y^2\right)\right. \\ &\quad \left. - \left(f_{xy} - \frac{2\|\boldsymbol{\alpha}\|^2}{M_T M_R \sigma^2}u_x u_y\right)^2\right) \end{aligned} \tag{27}$$

The CRB of the target coordinates is equal to the diagonal elements of the 3×3 top left submatrix of the inverse of the Fisher Information Matrix. Since the FIM has a block-diagonal structure, to obtain closed-form expressions of the CRBs, only the inverse of the matrix $\boldsymbol{Q}$ is needed.

The matrix $\boldsymbol{Q}$ is symmetric with respect to the main diagonal. The diagonal elements of the upper-left (3×3) submatrix are given by

$$f_{(p)(p)} = 2ND_{\mathrm{SNR}} \sum_{m=1}^{M_T}\sum_{n=1}^{M_R}\left(\frac{\partial \delta_m^{(T)}}{\partial(p)} + \frac{\partial \delta_n^{(R)}}{\partial(p)}\right)^2, \tag{28}$$

where (p) is to be replaced by the corresponding target location parameter x, y, or z, and $D_{\mathrm{SNR}} = \frac{\|\boldsymbol{\alpha}\|^2}{N\sigma^2}$. The off-diagonal elements are expressed as follows

$$f_{xy} = f_{yx} =$$

$$2ND_{\mathrm{SNR}}\sum_{m=1}^{M_T}\sum_{n=1}^{M_R}\left(\frac{\partial\delta_m^{(T)}}{\partial x}+\frac{\partial\delta_n^{(R)}}{\partial x}\right)\left(\frac{\partial\delta_m^{(T)}}{\partial y}+\frac{\partial\delta_n^{(R)}}{\partial y}\right), \tag{29}$$

$$f_{xz}=f_{zx}=$$

$$2ND_{\mathrm{SNR}}\sum_{m=1}^{M_T}\sum_{n=1}^{M_R}\left(\frac{\partial\delta_m^{(T)}}{\partial x}+\frac{\partial\delta_n^{(R)}}{\partial x}\right)\left(\frac{\partial\delta_m^{(T)}}{\partial z}+\frac{\partial\delta_n^{(R)}}{\partial z}\right), \tag{30}$$

$$f_{yz}=f_{zy}=$$

$$2ND_{\mathrm{SNR}}\sum_{m=1}^{M_T}\sum_{n=1}^{M_R}\left(\frac{\partial\delta_m^{(T)}}{\partial y}+\frac{\partial\delta_n^{(R)}}{\partial y}\right)\left(\frac{\partial\delta_m^{(T)}}{\partial z}+\frac{\partial\delta_n^{(R)}}{\partial z}\right). \tag{31}$$

The vectors $\boldsymbol{f}_{\boldsymbol{\psi}x}, \boldsymbol{f}_{x\boldsymbol{\psi}}^{\mathrm{T}}, \boldsymbol{f}_{\boldsymbol{\psi}y}, \boldsymbol{f}_{y\boldsymbol{\psi}}^{\mathrm{T}}, \boldsymbol{f}_{\boldsymbol{\psi}z}$ and $\boldsymbol{f}_{z\boldsymbol{\psi}}^{\mathrm{T}}$ of size $N\times 1$ are defined as

$$\boldsymbol{f}_{\boldsymbol{\psi}(p)}=\boldsymbol{f}_{(p)\boldsymbol{\psi}}^{\mathrm{T}}=-\frac{2}{\sigma^2}\underbrace{\sum_{m=1}^{M_T}\sum_{n=1}^{M_R}\left(\frac{\partial\delta_m^{(T)}}{\partial(p)}+\frac{\partial\delta_n^{(R)}}{\partial(p)}\right)}_{u_{(p)}}(\boldsymbol{\alpha}\odot\boldsymbol{\alpha}), \tag{32}$$

where again (p) is to be replaced by the corresponding target location parameter x, y, or z. The diagonal lower right matrix $\boldsymbol{F}_{\boldsymbol{\psi}}\in\mathbb{R}^{N\times N}$ is given by

$$\boldsymbol{F}_{\boldsymbol{\psi}}=\frac{2M_TM_R}{\sigma^2}\mathrm{diag}(\boldsymbol{\alpha}\odot\boldsymbol{\alpha}), \tag{33}$$

where $\odot$ denotes the Hadamard product. As it can be seen from the equations, the CRB is phase-invariant, i.e., it does not depend on the phases of the reflection coefficients in the matrix $\boldsymbol{D}$. For more details on the derivation of the above equations, we refer the reader to Appendix B.

Analytical inversion. We perform an analytical blockwise inversion of the matrix $\boldsymbol{Q}$ based on the fact that the lower right submatrix $\boldsymbol{F}_{\boldsymbol{\psi}}$ is diagonal.

We divide the matrix $\boldsymbol{Q}$ into the four blocks, as it is shown in (23), and define the Schur complement [42] of the matrix $\boldsymbol{F}_{\boldsymbol{\psi}}$:

$$\boldsymbol{S}=\boldsymbol{F}_{\boldsymbol{pp}}-\boldsymbol{F}_{\boldsymbol{p\psi}}\boldsymbol{F}_{\boldsymbol{\psi}}^{-1}\boldsymbol{F}_{\boldsymbol{\psi p}}. \tag{34}$$

As long as the matrix corresponding to the target parameters $\boldsymbol{F}_{\boldsymbol{pp}}$ is in the upper left block of the matrix $\boldsymbol{Q}$, only $\boldsymbol{F}_{\boldsymbol{\psi}}$ and the Schur complement require an inversion. The matrix $\boldsymbol{F}_{\boldsymbol{\psi}}$ is easily inverted as it is diagonal, and the Schur complement can be analytically inverted as a 3×3 matrix.

Finally, we obtain a non-matrix expression for the CRB in Cartesian coordinates of a single target, see equations (25), (26), and (27), where $\det(\boldsymbol{S})$ is the determinant of the 3×3 Schur complement matrix, and u_x, u_y, and u_z are given by

$$u_{(p)}=\sum_{m=1}^{M_T}\sum_{n=1}^{M_R}\left(\frac{\partial\delta_m^{(T)}}{\partial(p)}+\frac{\partial\delta_n^{(R)}}{\partial(p)}\right), \tag{35}$$

where (p) corresponds to the target location parameter x, y, or z. For the proof of (25), (26) and (27), and more details on the derivations, we refer the reader to Appendix C.

The obtained non-matrix expressions allow us to significantly reduce the computational cost of the CRB calculation and to analyse the potential performance of parameter estimation algorithms.

B. Unconditional Cramér-Rao Bound

The unconditional signal model assumes the signals to be random, i.e., the matrix of complex reflection coefficients $\boldsymbol{D}$ varies from realization to realization. We model the sequence of the reflection coefficients as a ZMCSCG random process with covariance matrix $\boldsymbol{R}_d=\mathbb{E}\{\boldsymbol{d}(k)\boldsymbol{d}(k)^{\mathrm{H}}\}$, where $\boldsymbol{d}(k)\in\mathbb{C}^H$ are the reflection coefficients at snapshot k. Then the received data $\boldsymbol{y}$ is a realization of a ZMCSCG process with covariance matrix $\boldsymbol{R}=(\boldsymbol{A}\diamond\boldsymbol{B})\boldsymbol{R}_d(\boldsymbol{A}\diamond\boldsymbol{B})^H+\sigma^2\boldsymbol{I}_{M_TM_R}$,

$$\boldsymbol{y}\sim\mathcal{CN}(\boldsymbol{0},\boldsymbol{R}). \tag{36}$$

1) General Case: First, let us consider the general case with multiple targets. The unconditional parameter vector is $\boldsymbol{\xi}=[\boldsymbol{p},\boldsymbol{\beta},\sigma^2]^{\mathrm{T}}\in\mathbb{R}^{(3H+\frac{(1+H)H}{2}+1)\times 1}$, where $\boldsymbol{\beta}$ is a $\frac{(1+H)H}{2}\times 1$ vector made from $\{[\boldsymbol{R}_d]_{ii}\}$ and $\{\angle\{[\boldsymbol{R}_d]_{ij}\},|[\boldsymbol{R}_d]_{ij})|$ for $j>i\}$, and $\boldsymbol{p}=[x_1,y_1,z_1,\ldots,x_H,y_H,z_H]^{\mathrm{T}}\in\mathbb{R}^{3H\times 1}$ is a vector of Cartesian coordinates of the targets. Again using (17) and the new parameter vector $\boldsymbol{\xi}$, the UFIM is expressed as follows:

$$[\mathbf{UFIM}(\boldsymbol{\xi})]_{ij}=N\mathrm{tr}\left[\boldsymbol{R}^{-1}\frac{\partial\boldsymbol{R}}{\partial\xi_i}\boldsymbol{R}^{-1}\frac{\partial\boldsymbol{R}}{\partial\xi_j}\right]. \tag{37}$$

Equation (38) on the top of the next page defines a matrix expression of the SCRB corresponding to the target location parameters. The derivation is according to [43]. The matrix $\boldsymbol{P}$ is defined as

$$\boldsymbol{P}=\left[\frac{\partial\boldsymbol{C}}{\partial x_1}\quad\frac{\partial\boldsymbol{C}}{\partial y_1}\quad\frac{\partial\boldsymbol{C}}{\partial z_1}\quad\cdots\frac{\partial\boldsymbol{C}}{\partial x_H}\quad\frac{\partial\boldsymbol{C}}{\partial y_H}\quad\frac{\partial\boldsymbol{C}}{\partial z_H}\right], \tag{42}$$

where $\boldsymbol{C}=(\boldsymbol{A}\diamond\boldsymbol{B})$, $\mathbf{1}_{3\times 3}=\mathbf{1}_3\mathbf{1}_3^{\mathrm{T}}$ is a matrix of ones, and $\boldsymbol{\Pi}=\boldsymbol{I}_{M_TM_R}-\boldsymbol{C}(\boldsymbol{C}^H\boldsymbol{C})^{-1}\boldsymbol{C}^H$. The SCRBs corresponding to the Cartesian coordinates of the targets are equal to the diagonal elements of the inverse of $[\mathbf{UFIM}(\boldsymbol{\xi})]_{1:3H,1:3H}$. For more details on the derivation of the UFIM in (38), we refer the reader to Appendix A.

2) One Target Case: Let us next consider a scenario with one target. The parameter vector is $\boldsymbol{\xi}=[x,y,z,\sigma_s^2,\sigma^2]^{\mathrm{T}}\in\mathbb{R}^{5\times 1}$, and, consequently, the unconditional CRB equation in (38) is then reduced to

$$[\mathbf{SCRB}(\boldsymbol{\xi})]_{1:3,1:3}=\frac{\sigma^2}{2\sigma_s^4N}\left[\Re\left\{\boldsymbol{c}^H\boldsymbol{R}^{-1}\boldsymbol{c}(\boldsymbol{P}^H\boldsymbol{\Pi}\boldsymbol{P})\right\}\right]^{-1}, \tag{43}$$

where $\boldsymbol{c}=(\boldsymbol{a}\diamond\boldsymbol{b})$, $\boldsymbol{P}=\left[\frac{\partial\boldsymbol{c}}{\partial x}\quad\frac{\partial\boldsymbol{c}}{\partial y}\quad\frac{\partial\boldsymbol{c}}{\partial z}\right]$, and $\boldsymbol{\Pi}=\boldsymbol{I}_{M_TM_R}-\frac{1}{M_TM_R}\boldsymbol{c}\boldsymbol{c}^H$. An inverse of the covariance matrix $\boldsymbol{R}$ is given by

$$\boldsymbol{R}^{-1}=(\sigma_s^2\boldsymbol{c}\boldsymbol{c}^H+\sigma^2\boldsymbol{I}_{M_TM_R})^{-1} \tag{44}$$

$$=\frac{1}{\sigma^2}\left(\boldsymbol{I}_{M_TM_R}-U_{\mathrm{SNR}}\frac{\boldsymbol{c}\boldsymbol{c}^H}{1+U_{\mathrm{SNR}}M_TM_R}\right). \tag{45}$$

The SCRB for Cartesian coordinates of the targets is equal to the diagonal elements of the $[\mathbf{SCRB}(\boldsymbol{\xi})]_{1:3,1:3}$.

$$[\mathbf{UFIM}(\boldsymbol{\xi})]_{1:3H,1:3H} = \frac{\sigma^2}{2\,N}\left[\Re\left\{(\boldsymbol{P}^H\boldsymbol{\Pi}\boldsymbol{P})\odot(\mathbf{1}_{3\times 3}\otimes\boldsymbol{R}_d\boldsymbol{C}^H\boldsymbol{R}^{-1}\boldsymbol{C}\boldsymbol{R}_d)^{\mathrm{T}}\right\}\right] \tag{38}$$

$$\mathrm{DCRB}(\rho) = \left(\frac{\partial\rho}{\partial x}\right)^2\mathrm{DCRB}(x) + \left(\frac{\partial\rho}{\partial y}\right)^2\mathrm{DCRB}(y) + \left(\frac{\partial\rho}{\partial z}\right)^2\mathrm{DCRB}(z) + 2\frac{\partial\rho}{\partial x}\frac{\partial\rho}{\partial y}\mathrm{DCRB}(xy) + 2\frac{\partial\rho}{\partial x}\frac{\partial\rho}{\partial z}\mathrm{DCRB}(xz) + + 2\frac{\partial\rho}{\partial y}\frac{\partial\rho}{\partial z}\mathrm{DCRB}(yz) \tag{39}$$

$$\mathrm{DCRB}(\phi) = \left(\frac{\partial\phi}{\partial x}\right)^2\mathrm{DCRB}(x) + \left(\frac{\partial\phi}{\partial y}\right)^2\mathrm{DCRB}(y) + 2\frac{\partial\phi}{\partial x}\frac{\partial\phi}{\partial y}\mathrm{DCRB}(xy), \tag{40}$$

$$\mathrm{DCRB}(\theta) = \left(\frac{\partial\theta}{\partial x}\right)^2\mathrm{DCRB}(x) + \left(\frac{\partial\theta}{\partial y}\right)^2\mathrm{DCRB}(y) + \left(\frac{\partial\theta}{\partial z}\right)^2\mathrm{DCRB}(z) + 2\frac{\partial\theta}{\partial x}\frac{\partial\theta}{\partial y}\mathrm{DCRB}(xy) + 2\frac{\partial\theta}{\partial x}\frac{\partial\theta}{\partial z}\mathrm{DCRB}(xz) + + 2\frac{\partial\theta}{\partial y}\frac{\partial\theta}{\partial z}\mathrm{DCRB}(yz), \tag{41}$$

C. Change of Variables

In the previous sections, the CRB has been derived with respect to the Cartesian coordinates of targets since they provide more convenient and straightforward expressions for the path differences and allow us to shift the origin of the system of coordinates without extra calculations. But there might be an interest to investigate the CRB regarding such physical parameters of the system as the range and the direction-of-arrival (DoA)/direction-of-departure (DoD). The lower bound on the variance, defined for the distance and the angles, is more informative and specific. Thus, it could be used, for instance, to analyse the estimation performance separately for ranges and angles.

In this section, we perform a transformation of the CRB corresponding to the Cartesian coordinates to the spherical coordinates of the targets, using the following change of variables formula [21]

$$\mathbf{CRB}(\boldsymbol{\kappa}) = \frac{\partial g(\boldsymbol{\xi})}{\partial\boldsymbol{\xi}}\mathbf{CRB}(\boldsymbol{\xi})\left[\frac{\partial g(\boldsymbol{\xi})}{\partial\boldsymbol{\xi}}\right]^{\mathrm{T}}, \tag{46}$$

where $\mathrm{CRB}(\boldsymbol{\xi})$ is the CRB matrix corresponding the Cartesian coordinate system, and $\mathbf{CRB}(\boldsymbol{\kappa})$ is a CRB defined with respect to the new parameter vector in spherical coordinates:

$$\boldsymbol{\kappa} = g(\boldsymbol{\xi}) = [\rho_1,\phi_1,\theta_1,\ldots,\rho_H,\phi_H,\theta_H,\mathrm{vec}(\boldsymbol{\psi}),\mathrm{vec}(\boldsymbol{\alpha}),\sigma^2]^{\mathrm{T}} \in \mathbb{R}^{P\times 1}, \tag{47}$$

where $\rho_h = \sqrt{x_h^2+y_h^2+z_h^2}$, $\phi_h = \arctan\frac{y_h}{x_h}$, and $\theta_h = \arcsin\frac{z_h}{x_h^2+y_h^2+z_h^2}$. Accordingly, the Jacobian matrix is defined as:

$$\frac{\partial g(\boldsymbol{\xi})}{\partial\boldsymbol{\xi}} = \mathrm{bdiag}(\boldsymbol{G}_1,\ldots,\boldsymbol{G}_H,\boldsymbol{I}_{2NH+1}) \in \mathbb{R}^{P\times P}, \tag{48}$$

where $\boldsymbol{G}_1,\ldots,\boldsymbol{G}_H$ are the (3×3) matrices containing the gradients of a vector of spherical targets coordinates, defined via x, y, and z, with respect to the corresponding Cartesian coordinates of the targets. Since the last block of $\frac{\partial g(\boldsymbol{\xi})}{\partial\boldsymbol{\xi}}$ is just an identity matrix, it can be dropped.

To calculate the CRB with respect to the new parameter vector $\boldsymbol{\kappa}$ in (47), we use the same equation (46) for both conditional and unconditional CRBs. In the first case, $\mathbf{CRB}(\boldsymbol{\xi})$ is replaced by $[\mathbf{DCRB}(\boldsymbol{\xi})]_{1:3H,1:3H}$, and by $[\mathbf{SCRB}(\boldsymbol{\xi})]_{1:3H,1:3H}$ in the unconditional system case. Then the CRBs for the range, azimuth, and elevation parameters of the targets are equal to the elements on the main diagonal of the $\mathbf{CRB}(\boldsymbol{\kappa})$.

Conditional model, one target scenario. For a system with one target, the new parameter vector in spherical coordinates is defined as

$$\boldsymbol{\kappa} = g(\boldsymbol{\xi}) = [\rho,\phi,\theta,\boldsymbol{\psi}^{\mathrm{T}},\boldsymbol{\alpha}^{\mathrm{T}},\sigma^2]^{\mathrm{T}} \in \mathbb{R}^{(2N+4)\times 1}. \tag{49}$$

To perform the conversion between the $\mathrm{CRB}(\boldsymbol{\xi})$ and $\mathrm{CRB}(\boldsymbol{\kappa})$ we use the change of variables formula (46). Since the difference between the two parameter vectors is only in the first three elements, the Jacobian matrix is given by

$$\frac{\partial g(\boldsymbol{\xi})}{\partial\boldsymbol{\xi}} = \mathrm{bdiag}(\boldsymbol{G},\boldsymbol{I}_{2N+1}) \in \mathbb{R}^{(2N+4)\times(2N+4)}, \tag{50}$$

where

$$\boldsymbol{G} = \begin{bmatrix} \frac{\partial\rho}{\partial x} & \frac{\partial\rho}{\partial y} & \frac{\partial\rho}{\partial z} \\ \frac{\partial\phi}{\partial x} & \frac{\partial\phi}{\partial y} & \frac{\partial\phi}{\partial z} \\ \frac{\partial\rho}{\partial x} & \frac{\partial\theta}{\partial y} & \frac{\partial\theta}{\partial z} \end{bmatrix}. \tag{51}$$

We refer the reader to Appendix C for the explicit expression of each element in $\boldsymbol{G}$.

The upper left (3×3) block of the matrix $\mathbf{CRB}(\boldsymbol{\xi})$ is equal to

$$\begin{bmatrix} \mathrm{DCRB}(x) & \mathrm{DCRB}(xy) & \mathrm{DCRB}(xz) \\ \mathrm{DCRB}(xy) & \mathrm{DCRB}(y) & \mathrm{DCRB}(yz) \\ \mathrm{DCRB}(xz) & \mathrm{DCRB}(yz) & \mathrm{DCRB}(z) \end{bmatrix}, \tag{52}$$

in which the elements of the main diagonal are presented in (25), (26), and (27), and the off-diagonal elements are calculated in a similar way (see (83), (84), and (85) in Appendix C). The non-matrix expressions of the conditional CRB for the range, azimuth, and elevation are defined in (39), (40), and (41) on the top of the previous page.

D. Resolution Limit for Two Closely-Spaced Targets

In this section, we investigate the minimum distance which is required to resolve two closely spaced targets. To determine the resolution limit we use the criterion proposed in [34], where the minimum resolvability distance d_{NF} is defined as the distance between two sources which is equal to the (minimum) standard deviation of the source separation or $\sqrt{\mathrm{CRB}(d_{\mathrm{NF}})}$. In other words, two targets are properly resolved if

$$\sqrt{\mathrm{CRB}(d_{\mathrm{NF}})} \leq d_{\mathrm{NF}}, \tag{53}$$

To find $\sqrt{\mathrm{CRB}(d_{\mathrm{NF}})}$, we extend the approach used in [33] to the 3-D bistatic MIMO radar system. In a 3-D space, the distance between two targets is defined as

$$d_{\mathrm{NF}} = \sqrt{(x_1 - x_2)^2 + (y_1 - y_2)^2 + (z_1 - z_2)^2}, \tag{54}$$

where x_1, x_2, y_1, y_2, z_1, and z_2 are the Cartesian coordinates of two targets with respect to the transmit or the receive array. Thus, the new unknown physical parameter vector is

$$\boldsymbol{j}(\boldsymbol{\xi}) = \left[d_{\mathrm{NF}}, y_1, z_1, x_2, y_2, z_2, \boldsymbol{\psi}_1^T, \boldsymbol{\psi}_2^T, \boldsymbol{\alpha}_1^T, \boldsymbol{\alpha}_2^T, \sigma^2\right]^T \tag{55}$$

for the conditional case, and

$$\boldsymbol{j}(\boldsymbol{\xi}) = [d_{\mathrm{NF}}, y_1, z_1, x_2, y_2, z_2, \boldsymbol{\beta}, \sigma^2]^{\mathrm{T}}, \tag{56}$$

where $\boldsymbol{\beta}$ is a $\frac{(1+H)H}{2} \times 1$ vector made from $\{[\boldsymbol{R}_d]_{ii}\}$ and $\{\angle\{[\boldsymbol{R}_d]_{ij}\}, |[\boldsymbol{R}_d]_{ij})|$ for $j > i\}$, for the the unconditional case. We obtain $\mathrm{CRB}(d_{\mathrm{NF}})$ by change of variables in the same manner as in (46)

$$\mathrm{CRB}\left(d_{\mathrm{NF}}\right) = \left[\frac{\partial \boldsymbol{j}(\boldsymbol{\xi})}{\partial \boldsymbol{\xi}} \mathrm{CRB}(\boldsymbol{\xi}) \left[\frac{\partial \boldsymbol{j}(\boldsymbol{\xi})}{\partial \boldsymbol{\xi}}\right]^T\right]_{1,1} \tag{57}$$

One can see from (43) that $\widehat{\mathrm{CRB}}(\boldsymbol{\xi}) = \frac{\mathrm{CRB}(\boldsymbol{\xi})}{\sigma^2}$ does not depend on σ^2. Therefore, using this definition of $\widehat{\mathrm{CRB}}(\boldsymbol{\xi})$ from [33] we can rewrite (57) as follows

$$\widehat{\mathrm{CRB}}(d_{\mathrm{NF}}) = \left[\frac{\partial \boldsymbol{j}(\boldsymbol{\xi})}{\partial \boldsymbol{\xi}} \widehat{\mathrm{CRB}}(\boldsymbol{\xi}) \left[\frac{\partial \boldsymbol{j}(\boldsymbol{\xi})}{\partial \boldsymbol{\xi}}\right]^T\right]_{1,1}. \tag{58}$$

Assuming ZMCSCG noise, we define the SNR as

$$\mathrm{SNR} = \frac{P_s}{\sigma^2}, \tag{59}$$

where P_s is the signal power. To properly resolve two targets the following equation holds [33]

$$\sigma^2 \widehat{\mathrm{CRB}}(d_{\mathrm{NF}}) \leq d_{\mathrm{NF}}^2. \tag{60}$$

Therefore, from (59) and (60) we obtain

$$\mathrm{SNR}_{\min} = \frac{P_s \widehat{\mathrm{CRB}}(d_{\mathrm{NF}})}{(x_1 - x_2)^2 + (y_1 - y_2)^2 + (z_1 - z_2)^2}. \tag{61}$$

Fig. 2 shows the minimum SNR required to resolve two closely spaced near-field targets with parameters $\rho_1 = \rho_2 = 5\lambda, \phi_1 = \phi_2 = 33^\circ, \theta_1 = 39$, and $\theta_2 = [39.01^\circ, \ldots, 42^\circ]$, where the resulting d_{NF} is calculated according to (54).

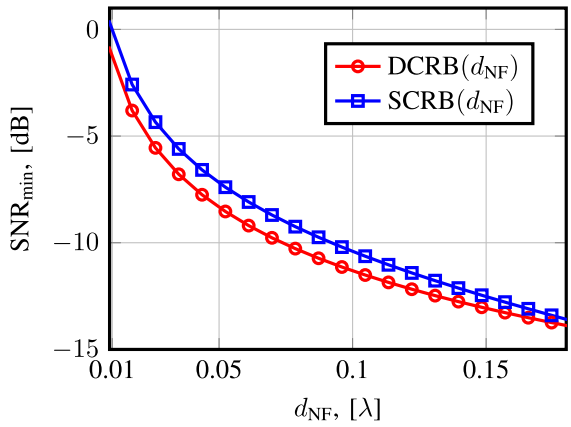

Fig. 2. $\mathrm{SNR}_{\min}$ vs. the distance between two targets.

TABLE I
TARGET PARAMETERS FOR THE SIMULATIONS IN FIG. 3

	ρ_T	ϕ_T	θ_T	ρ_R	ϕ_R	θ_R
$\boldsymbol{\Theta}_1^{(s)}$	4.46λ	33.69°	39.76°	3.61λ	121.18°	52.07°
$\boldsymbol{\Theta}_2^{(s)}$	4.8λ	33.69°	41.25°	3.87λ	116.57°	54.74°
$\boldsymbol{\Theta}_3^{(s)}$	4.84λ	31.1°	40.58°	3.78λ	114.1°	56.55°

IV. SIMULATION RESULTS

In the simulations, we consider a 3-D bistatic MIMO radar system with two URAs. Each array has $M_{T,x} = M_{R,x} = 4$ antennas along the x-axes and $M_{T,y} = M_{R,y} = 4$ antennas along the y-axes, so there are $M_T = M_R = 16$ antennas in the transmit and in the receive arrays. The reference receive antenna has the coordinates $x_R = 4\lambda, y_R = z_R = 0$ with respect to the transmit reference antenna, i.e., both antenna arrays are located in the x-y-plane as depicted in Fig. 1. The inter-element spacing is set to $d_T = d_R = \lambda/2$, where $\lambda = 1.5$ cm, and all the distances and errors in the simulation are normalized with respect to λ. We compute the CRBs separately for the transmit and receive side estimates. The matrix of the target reflection coefficients $\boldsymbol{D}$ is generated as a ZMCSCG process with variance $\sigma_s^2 = 1$ and varies from realization to realization in case of the unconditional model. In case of the conditional model, $\boldsymbol{D}$ is fixed for all realizations. Moreover, we introduce a correlation in the snapshot domain of the matrix $\boldsymbol{D}$ by employing the correlation matrix in which all off-diagonal elements are set to $\rho = 0.8$.

Estimation algorithms. In the first simulation, we compare the different target parameter estimation methods with the CRB. We change the SNR, which is defined as $1/\sigma^2$ and calculate the CRB for each parameter of the target. The number of snapshots is set to $N = 100$. We consider a difficult scenario with three closely spaced targets. The coordinates are depicted in Table I. The performance of the algorithms is evaluated in terms of the root mean square error (RMSE) in the following way

$$\mathrm{RMSE} = \sqrt{\frac{1}{T}\sum_{k=1}^{K}\sum_{h=1}^{H} \mathrm{I}_{k,h} \cdot (a_h - \hat{a}_{k,h})^2}, \tag{62}$$

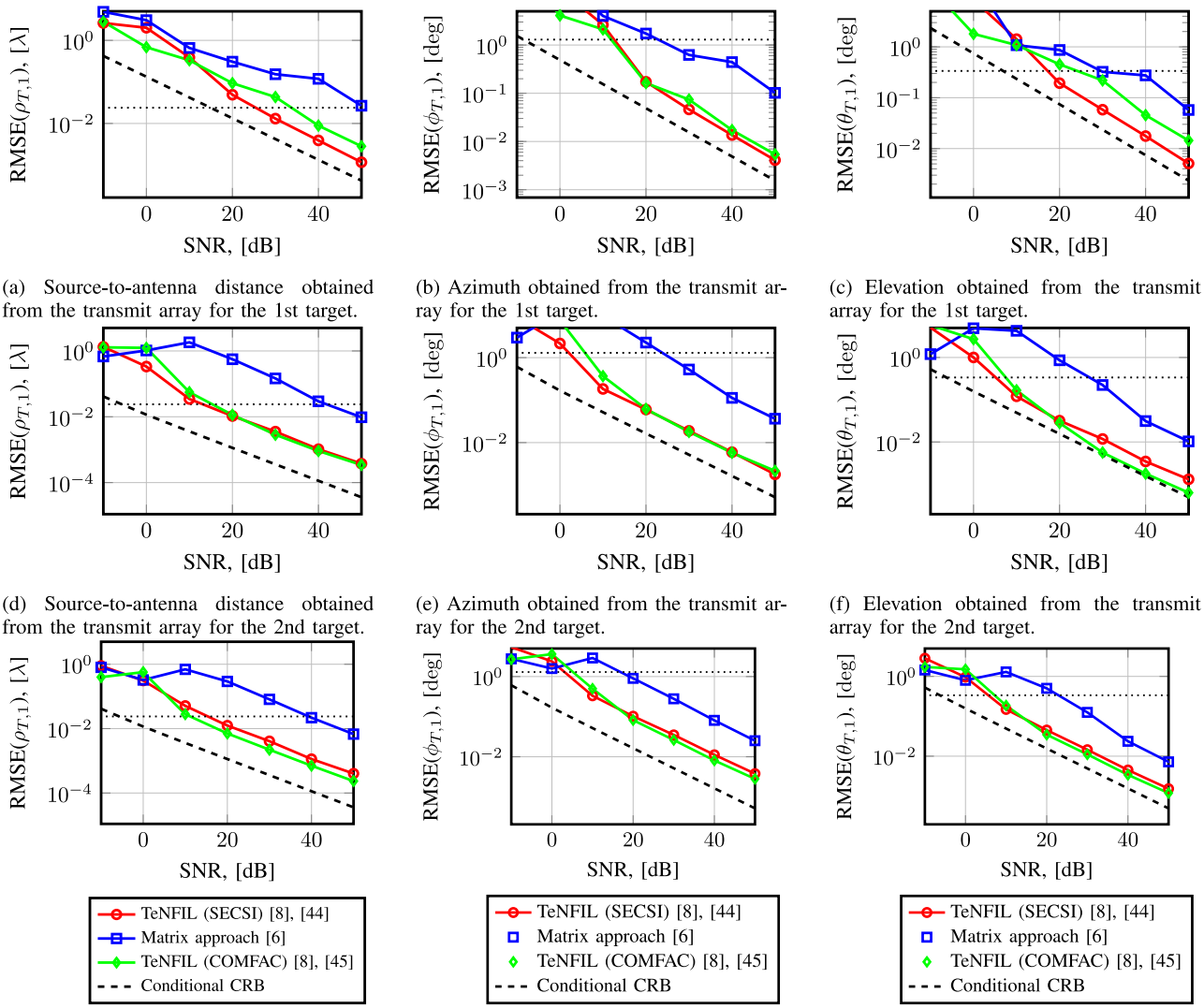

(a) Source-to-antenna distance obtained from the transmit array for the 1st target.
(b) Azimuth obtained from the transmit array for the 1st target.
(c) Elevation obtained from the transmit array for the 1st target.
(d) Source-to-antenna distance obtained from the transmit array for the 2nd target.
(e) Azimuth obtained from the transmit array for the 2nd target.
(f) Elevation obtained from the transmit array for the 2nd target.
(g) Source-to-antenna distance obtained from the transmit array for the 3rd target.
(h) Azimuth obtained from the transmit array for the 3rd target.
(i) Elevation obtained from the transmit array for the 3rd target.

Fig. 3. RMSE vs. SNR. Conditional CRB. $K = 3000$ trials. URA, $M_T = M_R = 16$, $H = 3$ radar targets.

$$T = \sum_{k=1}^{K} \sum_{h=1}^{H} \mathrm{I}_{k,h} \tag{63}$$

where $a_h \in \{\rho_{T,h}, \phi_{T,h}, \theta_{T,h}, \rho_{R,h}, \phi_{R,h}, \theta_{R,h}\}$, and $\hat{a}_{k,h}$ is an estimate of a_h in the k-th trial. We additionally apply the modulo-2π operator [36], [37] to the angle estimates to compute the circular error between the true and the estimated parameter. The quantity $\mathrm{I}_{k,h}$ denotes the indicator that the reliability test, applied to the angle estimates, has been passed, and T denotes the total number of cases, where the reliability test has not failed. The reliability test is applied in the parameter extraction part of the algorithms: if the argument of the $\cos^{-1}$ is smaller than 1, the reliability test has been passed and $\mathrm{I}_{k,h} = 1$. We set $\mathrm{I}_{k,h} = 0$ otherwise. For more details, we refer the reader to [8].

The simulation results for all three targets are depicted in Fig. 3. The red curves show the performance of the SECSI [44] based TeNFiL algorithm [8], the blue curves show the performance of the estimation algorithm proposed in [6] (denoted as "Matrix approach"), and the green curves depict the performance of the TeNFiL method that uses the ALS-based COMFAC algorithm [45] to compute the approximate CP decomposition of the received signal $\boldsymbol{\mathcal{Y}}$, also applied in [2] (instead of the SECSI framework). The dotted lines denote half of the smallest separation distance $\frac{d_s}{2}$ between the targets, where d_s is calculated as $d_s = \min\{a_i - a_j\}$, and a_h is one of the parameters from $\{\rho_{T,h}, \phi_{T,h}, \theta_{T,h}, \rho_{R,h}, \phi_{R,h}, \theta_{R,h}\}, i, j \in 1 \dots H$, and $i \neq j$. An error below that line indicates that two targets are properly resolved. We compare the errors, defined as in (62), with $\sqrt{\mathrm{CRB}(a_h)}$. As it can be observed from Fig. 3, the TeNFiL algorithm significantly outperforms the matrix approach from [6] and is close to the CRB for sufficiently high SNRs. In the chosen scenario, the SECSI and ALS based COMFAC algorithms for the estimation of the steering matrices show a similar performance at low SNRs, but the second algorithm is computationally less efficient due to the iterative nature and its execution time varies depending on the SNR. We can observe that the

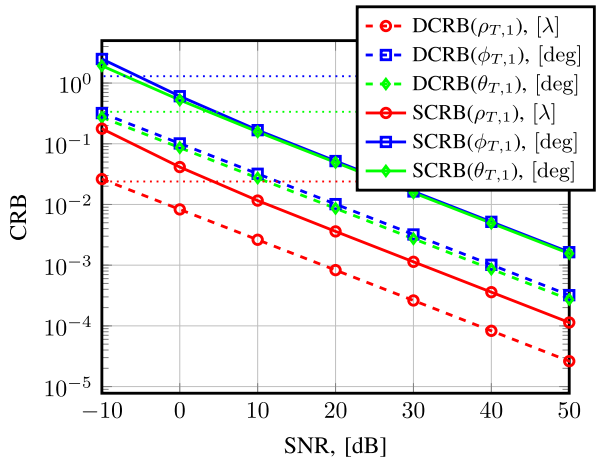

(a) CRB vs. SNR. Conditional (DCRB) and unconditional (SCRB) Cramér-Rao bound. Spherical coordinates.

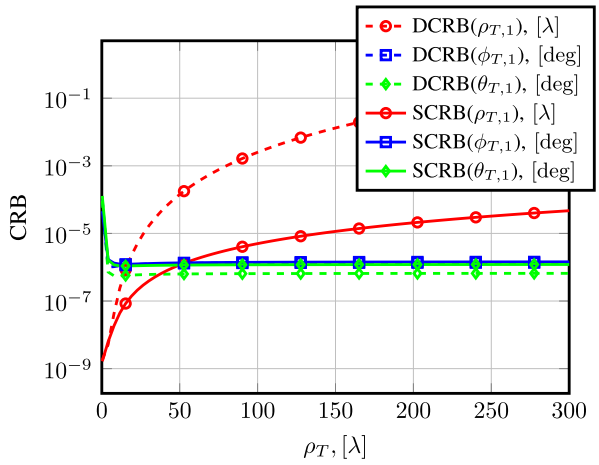

(b) CRB vs. Range. Conditional (DCRB) and unconditional (SCRB) Cramér-Rao bound. Spherical coordinates. SNR = 30 dB.

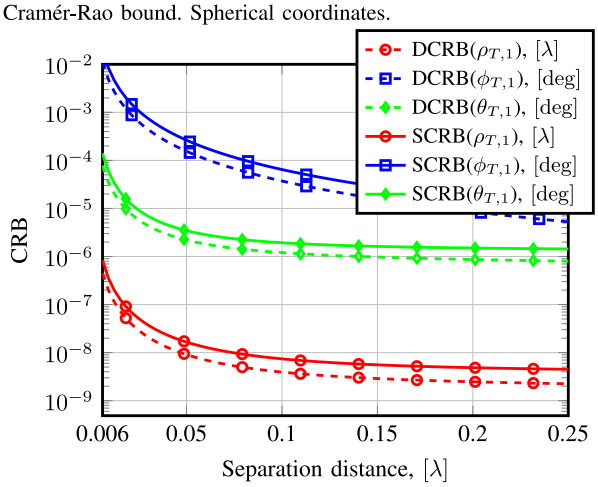

(c) CRB vs. Separation distance. Conditional (DCRB) and unconditional (SCRB) Cramér-Rao bound. Spherical coordinates. SNR = 30 dB.

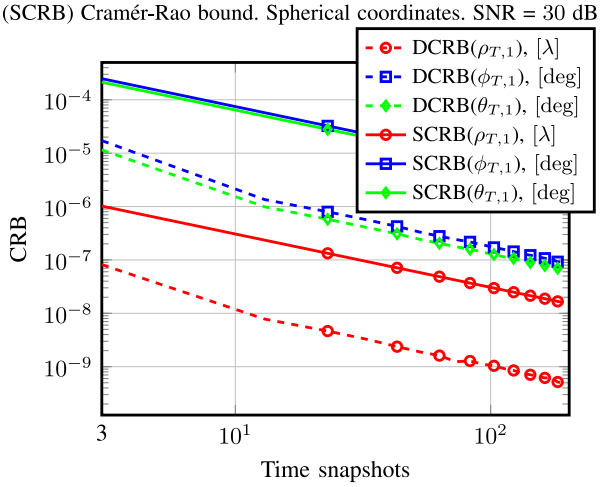

(d) CRB vs. Snapshots. Conditional (DCRB) and unconditional (SCRB) Cramér-Rao bound. Spherical coordinates. SNR = 30 dB.

Fig. 4. CRB vs. SNR (a), Range (b), Separation distance (c), and Snapshots (d).

TeNFiL performance is closer to the CRB, which is explained by the fact that the targets in the scenario are closely spaced, and in such a challenging scenario, tensor approach shows a better performance. The TeNFIL performance approaches the CRB for the elevation (Figures 3(c), 3(f), and 3(i)) due to the bigger resolution between the targets in terms of the elevation angles.

In the second simulation, we evaluate the behavior of the Conditional and Unconditional CRB by varying the parameters of the system such as SNR, range, distances between targets, and the number of snapshots.

SNR. Fig. 4(a) shows the conditional (dashed lines) and unconditional (solid lines) CRBs for the range, azimuth, and elevation estimates of the first target obtained from the transmit side. The target coordinates are depicted in Table I. The figure shows that the conditional CRB is smaller than the unconditional CRB. The bigger error for the azimuth angels is explained by their smaller separation distance. The dotted lines denote the half of the smallest separation distance between the targets. The two targets are properly resolved if the estimation error value is below that line. We can observe that in case of the deterministic model, $\mathrm{SNR} = -10\,\mathrm{dB}$ is enough to resolve the two closely spaced targets. The unconditional model requires higher values of the SNR in the same scenario.

TABLE II
TARGET PARAMETERS FOR THE SIMULATIONS IN FIG. 4(B)

	ρ_T	ϕ_T	θ_T	ρ_R	ϕ_R	θ_R
$\Theta_1^{(s)}$	0.3λ...300λ	$40°$	$40°$	changing accordingly		
$\Theta_2^{(s)}$	4λ	$-45°$	$45°$	4λ	$-135°$	$45°$

Range. In this simulation, we evaluate the estimation performance as a function of the range of the 1st target. We consider a scenario with two targets, where the position of the second target is fixed, while the first target is moving. The distance between the first target and the transmit array is changing from 0.3λ to 300λ, and the azimuth and elevation angles are fixed. The simulation results are depicted in Fig. 4(b). The target parameters are provided in Table II. The SNR is set to $\mathrm{SNR} = 30\,\mathrm{dB}$.

Fig. 4(b) demonstrates the performance of the conditional and the unconditional CRB for the first target, and the parameters

TABLE III
TARGET PARAMETERS FOR THE SIMULATIONS IN FIG. 4(C)

	ρ_T	ϕ_T	θ_T
$\boldsymbol{\Theta}_1^{(s)}$	changing according to $\boldsymbol{\Theta}_1^{(c)}$		
$\boldsymbol{\Theta}_2^{(s)}$	3.94λ	-9.5°	39.4°
	x_T	y_T	z_T
$\boldsymbol{\Theta}_1^{(c)}$	3λ	$-0.506\lambda ... -0.75\lambda$	2.5λ
$\boldsymbol{\Theta}_2^{(c)}$	3λ	-0.5λ	2.5λ

of the second target are constant. The red curves represent the CRB for the range, while the blue and green curves show the lower bounds for the azimuth and elevation, respectively. With the increasing distance, the error for the range is also increasing, whereas the CRB for the azimuth and elevation angles stays constant. The difference between the conditional and unconditional CRB becomes more significant with increasing range. These results provide a criterion to define the near-field region.

Separation distance. For the next simulation, we change the Euclidean distance between the targets in order to assess the minimum distance, which is required for targets to be properly resolved for a given SNR. The second target position is fixed, and the y coordinate of the 1st target changes: it moves away from the second target along the y-axis, such that both targets stay in the middle between the two arrays. In contrast with the previous simulation, all three spherical parameters (range, azimuth, and elevation) change. The coordinates are depicted in Table III. The SNR is fixed and equal to $\mathrm{SNR} = 30\,\mathrm{dB}$. The simulation results are shown in Fig. 4(c). This figure depicts the errors, calculated at the transmit side for the first target. For the receive side, the results are similar due to the symmetry of the scenario.

Number of snapshots. In this simulation, we investigate the dependence of the CRB on the number of snapshots. The target parameters are depicted in Table I, and the simulation results for the transmit side estimates in spherical coordinates are depicted in Fig. 4(d). The CRB gets smaller with an increasing number of snapshots since more information about the targets can be extracted when more samples are taken into account.

V. CONCLUSION

In this paper, the conditional and unconditional Cramér-Rao bounds have been derived for near-field bistatic MIMO radar systems. For the one target case, we provide the analytical inversion of the Fisher Information Matrix and, consequently, the non-matrix closed-form expressions of the CRB corresponding to Cartesian coordinates of the target locations. Additionally, the lower bounds for the target location parameters, defined in a spherical coordinate system, are obtained by the change of variables method. We have employed the derived CRBs to evaluate the performance of state-of-the-art target parameter estimation methods. Moreover, the CRB is used to analyse the minimum distance, which is required to properly resolve two closely spaced targets, and the impact of the target position on the estimation accuracy is investigated. Simulation results have shown that with an increasing antenna-to-target distance, the error in the range estimation also grows, whereas for the azimuth and elevation angles it stays constant.

APPENDIX A
DERIVATION OF THE ELEMENTS OF CFIM AND UFIM IN (19) AND (38)

In this appendix, we provide more details on the derivations of the conditional and unconditional FIMs in the multi-target case.

Conditional FIM.

The structure of the FIM in (19) follows the definition of the parameter vector in (18). Each element of the FIM in (19) is computed according to (17). The block of the FIM that corresponds to the target locations consists of the following 3×3 block matrices

$$\boldsymbol{F}_{\boldsymbol{pp}} = \begin{bmatrix} \boldsymbol{F}_{\boldsymbol{p}_1\boldsymbol{p}_1} & \cdots & \boldsymbol{F}_{\boldsymbol{p}_1\boldsymbol{p}_H} \\ \vdots & & \vdots \\ \boldsymbol{F}_{\boldsymbol{p}_H\boldsymbol{p}_1} & \cdots & \boldsymbol{F}_{\boldsymbol{p}_H\boldsymbol{p}_H} \end{bmatrix}, \tag{64}$$

where

$$\boldsymbol{F}_{\boldsymbol{p}_i\boldsymbol{p}_j} = \begin{bmatrix} f_{x_ix_j} & f_{x_iy_j} & f_{x_iz_j} \\ f_{y_ix_j} & f_{y_iy_j} & f_{y_iz_j} \\ f_{z_ix_j} & f_{z_iy_j} & f_{z_iz_j} \end{bmatrix}, i, j \in \{1 \dots H\}. \tag{65}$$

Each element of (65) is calculated as

$$\begin{aligned} f_{(p_h)(p_h)} &= \frac{2}{\sigma^2}\Re\left\{\frac{\partial \boldsymbol{\mu}^H}{\partial(p_h)}\frac{\partial \boldsymbol{\mu}}{\partial(p_h)}\right\} \\ &= \frac{2}{\sigma^2}\Re\left\{\sum_{k=1}^{N} d_{k,h}^* d_{k,h} \sum_{m=1}^{M_T}\sum_{n=1}^{M_R}\left(\frac{\partial a_{m,h}^*}{\partial(p_h)} b_{n,h}^* + \frac{\partial b_{n,h}^*}{\partial(p_h)} a_{m,h}^*\right)\right. \\ &\qquad \left.\cdot\left(\frac{\partial a_{m,h}}{\partial(p_h)} b_{n,h} + \frac{\partial b_{n,h}}{\partial(p_h)} a_{m,h}\right)\right\}, \end{aligned} \tag{66}$$

where (p_h) corresponds to the target location parameters x_h, y_h, or z_h, and

$$\boldsymbol{\mu} = (\boldsymbol{D} \diamond \boldsymbol{B} \diamond \boldsymbol{A})\mathbf{1}_H = \underbrace{\begin{bmatrix} \sum_{i=1}^{H} a_{1,i} b_{1,i} d_{1,i} \\ \vdots \\ \sum_{i=1}^{H} a_{M_T,i} b_{M_R,i} d_{1,i} \\ \vdots \\ \sum_{i=1}^{H} a_{1,i} b_{1,i} d_{N,i} \\ \vdots \\ \sum_{i=1}^{H} a_{M_T,i} b_{M_R,i} d_{N,i} \end{bmatrix}}_{\in \mathbb{C}^{M_T M_R N \times 1}} \tag{67}$$

Unconditional FIM.

According to (37), the UFIM is calculated as

$$[\mathbf{UFIM}(\boldsymbol{\xi})]_{ij} = N\mathrm{tr}\left[\boldsymbol{R}^{-1}\frac{\partial \boldsymbol{R}}{\partial \xi_i}\boldsymbol{R}^{-1}\frac{\partial \boldsymbol{R}}{\partial \xi_j}\right], \tag{68}$$

where

$$\boldsymbol{R} = (\boldsymbol{A} \diamond \boldsymbol{B})\boldsymbol{R}_d(\boldsymbol{A} \diamond \boldsymbol{B})^H + \sigma^2 \boldsymbol{I}_{M_T M_R}. \tag{69}$$

The following formula for the unconditional CRB of the parameter θ has been shown in [46]

$$\mathbf{SCRB}(\theta) = \frac{\sigma^2}{2\,N}\left[\Re\left\{(\boldsymbol{P}^H\boldsymbol{\Pi}\boldsymbol{P})\odot\boldsymbol{H}^{\mathrm{T}}\right\}\right]^{-1}, \tag{70}$$

Taking into account the parameter vector $\boldsymbol{\xi} = [\boldsymbol{p}, \boldsymbol{\beta}, \sigma^2]^{\mathrm{T}} \in \mathbb{R}^{(3H+\frac{(1+H)H}{2}+1)\times 1}$, where $\boldsymbol{\beta}$ is a $\frac{(1+H)H}{2}\times 1$ vector made from $\{[\boldsymbol{R}_d]_{ii}\}$ and $\{\angle\{[\boldsymbol{R}_d]_{ij}\}, |[\boldsymbol{R}_d]_{ij}| \text{ for } j>i\}$, the covariance matrix in (69), and following the derivations in [46], we get

$$\boldsymbol{H} = \mathbf{1}_{3\times 3}\otimes\left(\boldsymbol{R}_d\boldsymbol{C}^H\boldsymbol{R}^{-1}\boldsymbol{C}\boldsymbol{R}_d\right), \tag{71}$$

$$\boldsymbol{P} = \left[\frac{\partial\boldsymbol{C}}{\partial x_1}\quad\frac{\partial\boldsymbol{C}}{\partial y_1}\quad\frac{\partial\boldsymbol{C}}{\partial z_1}\quad\cdots\frac{\partial\boldsymbol{C}}{\partial x_H}\quad\frac{\partial\boldsymbol{C}}{\partial y_H}\quad\frac{\partial\boldsymbol{C}}{\partial z_H}\right] \in \mathbb{C}^{M_TM_R\times 3H}, \tag{72}$$

where $\boldsymbol{\Pi} = \boldsymbol{I}_{M_TM_R} - \boldsymbol{C}(\boldsymbol{C}^H\boldsymbol{C})^{-1}\boldsymbol{C}^H$, $\boldsymbol{C} = \boldsymbol{A}\diamond\boldsymbol{B}$, and $\boldsymbol{R}_d$ is the signal covariance matrix.

Appendix B
Derivation of the Elements of $\boldsymbol{Q}$ in (23)

In the following, we present the main steps which lead to the obtained closed-form CRB equations for a special case of one target, i.e., $H=1$. The signal mean $\boldsymbol{\mu}$ is defined as

$$\boldsymbol{\mu} = \boldsymbol{d}\diamond\boldsymbol{b}\diamond\boldsymbol{a} \in \mathbb{C}^{M_TM_RN\times 1}, \tag{73}$$

where $a_m = e^{-j\delta_m^{(T)}}, m=1,\ldots,M_T$, $b_n = e^{-j\delta_n^{(R)}}, n=1,\ldots,M_R$, $d_k = \alpha(k)e^{j\psi(k)}, k=1,\ldots,N$. Based on the general formula of the FIM, we derive $f_{(p)(p)}$, where (p) corresponds to the target location parameter x, y, or z, as follows

$$\begin{aligned} f_{(p)(p)} &= \frac{2}{\sigma^2}\Re\left\{\frac{\partial\boldsymbol{\mu}^H}{\partial(p)}\frac{\partial\boldsymbol{\mu}}{\partial(p)}\right\} \\ &= \frac{2}{\sigma^2}\Re\left\{\sum_{k=1}^{N} d_k^* d_k \sum_{m=1}^{M_T}\sum_{n=1}^{M_R}\left(\frac{\partial a_m^*}{\partial(p)}b_n^* + \frac{\partial b_n^*}{\partial(p)}a_m^*\right)\cdot \right. \\ &\qquad \left.\cdot\left(\frac{\partial a_m}{\partial(p)}b_n + \frac{\partial b_n}{\partial(p)}a_m\right)\right\}. \end{aligned} \tag{74}$$

Substituting a_m, b_n, and d_k according to (4), (5), and (3), and taking into account that $\frac{\partial(e^{-j\delta})}{\partial(p)} = -je^{-j\delta}(\frac{\partial\delta}{\partial(p)})$, we get

$$\begin{aligned} f_{(p)(p)} &= \frac{2}{\sigma^2}\sum_{k=1}^{N}\alpha_k^2\sum_{m=1}^{M_T}\sum_{n=1}^{M_R}\left(\frac{\partial\delta_m^{(T)}}{\partial(p)} + \frac{\partial\delta_n^{(R)}}{\partial(p)}\right)^2 \\ &= \frac{2}{\sigma^2}\|\boldsymbol{\alpha}\|^2\sum_{m=1}^{M_T}\sum_{n=1}^{M_R}\left(\frac{\partial\delta_m^{(T)}}{\partial(p)} + \frac{\partial\delta_n^{(R)}}{\partial(p)}\right)^2, \end{aligned} \tag{75}$$

$$\begin{aligned} f_{xy} = f_{yx} &= \frac{2}{\sigma^2}\Re\left\{\frac{\partial\boldsymbol{\mu}^H}{\partial x}\frac{\partial\boldsymbol{\mu}}{\partial y}\right\} \\ &= \frac{2}{\sigma^2}\Re\left\{\sum_{k=1}^{N} d_k^* d_k \sum_{m=1}^{M_T}\sum_{n=1}^{M_R}\left(\frac{\partial a_m^*}{\partial x}b_n^* + \frac{\partial b_n^*}{\partial x}a_m^*\right)\cdot \right. \\ &\qquad \left.\cdot\left(\frac{\partial a_m}{\partial y}b_n + \frac{\partial b_n}{\partial y}a_m\right)\right\} \\ &= \frac{2}{\sigma^2}\sum_{k=1}^{N}\alpha_k^2\sum_{m=1}^{M_T}\sum_{n=1}^{M_R}\left(\frac{\partial\delta_m^{(T)}}{\partial x} + \frac{\partial\delta_n^{(R)}}{\partial x}\right)\cdot \\ &\qquad \cdot\left(\frac{\partial\delta_m^{(T)}}{\partial y} + \frac{\partial\delta_n^{(R)}}{\partial y}\right) \\ &= \frac{2}{\sigma^2}\|\boldsymbol{\alpha}\|^2\sum_{m=1}^{M_T}\sum_{n=1}^{M_R}\left(\frac{\partial\delta_m^{(T)}}{\partial x} + \frac{\partial\delta_n^{(R)}}{\partial x}\right)\cdot \\ &\qquad \cdot\left(\frac{\partial\delta_m^{(T)}}{\partial y} + \frac{\partial\delta_n^{(R)}}{\partial y}\right). \end{aligned} \tag{76}$$

The other cross terms, f_{xz}, f_{zx}, f_{yz}, and f_{zy} are computed in a similar way as f_{xy}. The remaining terms are as follows:

$$\begin{aligned} f_{\psi_k(p)} = f_{(p)\psi_k} &= \frac{2}{\sigma^2}\Re\left\{\frac{\partial\boldsymbol{\mu}^H}{\partial\psi_k}\frac{\partial\boldsymbol{\mu}}{\partial(p)}\right\} \\ &= \frac{2}{\sigma^2}\Re\left\{d_k\frac{\partial d_k^*}{\partial\psi_k}\sum_{m=1}^{M_T}\sum_{n=1}^{M_R}a_m^*b_n^*\left(\frac{\partial a_m}{\partial(p)}b_n + \frac{\partial b_n}{\partial(p)}a_m\right)\right\}, \\ &\forall k = 1\ldots N, \end{aligned} \tag{77}$$

$$\boldsymbol{f}_{\boldsymbol{\psi}(p)} = \boldsymbol{f}_{(p)\boldsymbol{\psi}}^{\mathrm{T}} = -\frac{2}{\sigma^2}\sum_{m=1}^{M_T}\sum_{n=1}^{M_R}\left(\frac{\partial\delta_m^{(T)}}{\partial(p)} + \frac{\partial\delta_n^{(R)}}{\partial(p)}\right)(\boldsymbol{\alpha}\odot\boldsymbol{\alpha}), \tag{78}$$

$$F_{\psi_k\psi_k} = \frac{2}{\sigma^2}\Re\left\{\frac{\partial d_k}{\partial\psi_k^*}\frac{\partial d_k}{\partial\psi_k}\sum_{m=1}^{M_T}\sum_{n=1}^{M_R}a_m^*b_n^*a_mb_n\right\}, \tag{79}$$

$$F_{\psi_i\psi_j} = 0, \forall i\neq j, \tag{80}$$

$$\boldsymbol{F}_{\boldsymbol{\psi}\boldsymbol{\psi}} = \frac{2M_TM_R}{\sigma^2}\mathrm{diag}(\boldsymbol{\alpha}\odot\boldsymbol{\alpha}). \tag{81}$$

Appendix C
Analytical Inversion of $\boldsymbol{Q}$ in (23)

For the blockwise inversion of $\boldsymbol{Q}$ in (23), we divide $\boldsymbol{Q}$ into the four blocks in the following way

$$\begin{aligned} \boldsymbol{Q}^{-1} &= \left[\begin{array}{ccc|c} f_{xx} & f_{xy} & f_{xz} & \boldsymbol{f}_{x\boldsymbol{\psi}}^{\mathrm{T}} \\ f_{yx} & f_{yy} & f_{yz} & \boldsymbol{f}_{y\boldsymbol{\psi}}^{\mathrm{T}} \\ f_{zx} & f_{zy} & f_{zz} & \boldsymbol{f}_{z\boldsymbol{\psi}}^{\mathrm{T}} \\ \hline \boldsymbol{f}_{\boldsymbol{\psi}x} & \boldsymbol{f}_{\boldsymbol{\psi}y} & \boldsymbol{f}_{\boldsymbol{\psi}z} & \boldsymbol{F}_{\boldsymbol{\psi}\boldsymbol{\psi}} \end{array}\right]^{-1} \\ &= \left[\begin{array}{c|c} \boldsymbol{A} & \boldsymbol{B} \\ \hline \boldsymbol{C} & \boldsymbol{F} \end{array}\right]^{-1} \\ &= \left[\begin{array}{c|c} \boldsymbol{S}^{-1} & -\boldsymbol{S}^{-1}\boldsymbol{B}\boldsymbol{F}^{-1} \\ \hline -\boldsymbol{F}^{-1}\boldsymbol{C}\boldsymbol{S}^{-1} & \boldsymbol{F}^{-1}+\boldsymbol{F}^{-1}\boldsymbol{C}\boldsymbol{S}^{-1}\boldsymbol{B}\boldsymbol{F}^{-1} \end{array}\right], \end{aligned} \tag{82}$$

where $\boldsymbol{S} = (\boldsymbol{A} - \boldsymbol{B}\boldsymbol{F}^{-1}\boldsymbol{C})$ is the Schur complement of the matrix $\boldsymbol{F}$. Using equations (32) and (33), we get

$$\begin{aligned}
\boldsymbol{B}\boldsymbol{F}^{-1}\boldsymbol{C} &= \underbrace{\begin{bmatrix} \boldsymbol{f}_{\psi x}^T \\ \boldsymbol{f}_{\psi y}^T \\ \boldsymbol{f}_{\psi z}^T \end{bmatrix}}_{3\times N} \underbrace{\boldsymbol{F}_{\psi\psi}^{-1}}_{N\times N} \underbrace{\begin{bmatrix} \boldsymbol{f}_{\psi x} & \boldsymbol{f}_{\psi y} & \boldsymbol{f}_{\psi z} \end{bmatrix}}_{N\times 3} \\
&= \frac{2}{M_T M_R \sigma^2} \begin{bmatrix} u_x \boldsymbol{\alpha}'^T \\ u_y \boldsymbol{\alpha}'^T \\ u_z \boldsymbol{\alpha}'^T \end{bmatrix} \begin{bmatrix} \frac{1}{\alpha_1^2} & & \\ & \ddots & \\ & & \frac{1}{\alpha_N^2} \end{bmatrix} \\
&\quad \begin{bmatrix} u_x \boldsymbol{\alpha}' & u_y \boldsymbol{\alpha}' & u_z \boldsymbol{\alpha}' \end{bmatrix} \\
&= \frac{2}{M_T M_R \sigma^2} \boldsymbol{u}\boldsymbol{\alpha}'^T (\mathrm{diag}\{\boldsymbol{\alpha}'\})^{-1} \boldsymbol{\alpha}' \boldsymbol{u}^T \\
&= \frac{2}{M_T M_R \sigma^2} \boldsymbol{u} \underbrace{\boldsymbol{1}^T \boldsymbol{\alpha}'}_{\|\boldsymbol{\alpha}\|^2} \boldsymbol{u}^T \\
&= \frac{2\|\boldsymbol{\alpha}\|^2}{M_T M_R \sigma^2} \begin{bmatrix} u_x u_x & u_x u_y & u_x u_z \\ u_y u_x & u_y u_y & u_y u_z \\ u_z u_x & u_z u_y & u_z u_z \end{bmatrix},
\end{aligned}$$

where $\boldsymbol{u} = \begin{bmatrix} u_x & u_y & u_z \end{bmatrix}^T$ and $\boldsymbol{\alpha}' = \boldsymbol{\alpha} \odot \boldsymbol{\alpha} \in \mathbb{R}^{N\times 1}$. Using the definition of $\boldsymbol{A}$ in (82), the inverse of $\boldsymbol{S}$ can be written as

$$\boldsymbol{S}^{-1} = \begin{bmatrix} f_{xx} - v u_x^2 & f_{xy} - v u_x u_y & f_{xz} - v u_x u_z \\ f_{yx} - v u_x u_y & f_{yy} - v u_y^2 & f_{yz} - v u_y u_z \\ f_{zx} - v u_x u_z & f_{zy} - v u_y u_z & f_{zz} - v u_z^2 \end{bmatrix}^{-1}, \tag{86}$$

where $v = \frac{2\|\boldsymbol{\alpha}\|^2}{M_T M_R \sigma^2}$. The matrix $\boldsymbol{S}$ can be inverted as a 3×3 matrix

$$\boldsymbol{S}^{-1} = \begin{bmatrix} a & b & c \\ d & e & f \\ g & h & i \end{bmatrix}^{-1} = \frac{1}{\det(\boldsymbol{S})} \begin{bmatrix} A & D & G \\ B & E & H \\ C & F & I \end{bmatrix}, \tag{87}$$

and $A = (ei - fh),\ B = -(di - fg),\ C = (dh - eg),\ D = -(bi - ch), E = (ai - cg), F = -(ah - bg), G = (bf - ce), H = -(af - cd), I = (ae - bd)$. Moreover, the determinant of $\boldsymbol{S}$ is given by

$$\det(\boldsymbol{S}) = aei + bfg + cdh - ceg - bdi - afh. \tag{88}$$

Using equations (86) and (87), $\det(\boldsymbol{S})$ in (88) can be rewritten as

$$\begin{aligned}
\det(\boldsymbol{S}) = \frac{2\|\boldsymbol{\alpha}\|^2}{M_T M_R \sigma^2} &(f_{yz}^2 u_x^2 - f_{yy} f_{zz} u_x^2 + 2 f_{zz} f_{xy} u_x u_y \\
&- 2 f_{xz} f_{yz} u_x u_y - 2 f_{xy} f_{yz} u_x u_z + 2 f_{yy} f_{xz} u_x u_z \\
&+ f_{xz}^2 u_y^2 - f_{xx} f_{zz} u_y^2 - 2 f_{xy} f_{xz} u_y u_z \\
&+ 2 f_{xx} f_{yz} u_y u_z + f_{xy}^2 u_z^2 - f_{xx} f_{yy} u_z^2) \\
&- f_{zz} f_{xy}^2 + 2 f_{xy} f_{xz} f_{yz} - f_{yy} f_{xz}^2 - f_{xx} f_{yz}^2 \\
&+ f_{xx} f_{yy} f_{zz}.
\end{aligned} \tag{89}$$

Using the definitions in (87), the CRBs for x, y, and z are equal to the corresponding diagonal elements of the inverse of the Schur complement:

$$\mathrm{DCRB}(x) = \frac{1}{\det(\boldsymbol{S})} A, \qquad \mathrm{DCRB}(y) = \frac{1}{\det(\boldsymbol{S})} E,$$
$$\mathrm{DCRB}(z) = \frac{1}{\det(\boldsymbol{S})} I.$$

We also define the cross terms of the inverse of the Schur complement, since they are used in the derivations of the CRB corresponding to the spherical coordinates of the targets:

$$\mathrm{DCRB}(xy) = \frac{1}{\det(\boldsymbol{S})} D, \qquad \mathrm{DCRB}(xz) = \frac{1}{\det(\boldsymbol{S})} G,$$
$$\mathrm{DCRB}(yz) = \frac{1}{\det(\boldsymbol{S})} H.$$

The cross terms in (52) are given in equations (83), (84), and (85) on the bottom of previous page, and the matrix $\boldsymbol{G}$ in (51) is given as

$$\begin{bmatrix} \frac{\partial\rho}{\partial x} & \frac{\partial\rho}{\partial y} & \frac{\partial\rho}{\partial z} \\ \frac{\partial\phi}{\partial x} & \frac{\partial\phi}{\partial y} & \frac{\partial\phi}{\partial z} \\ \frac{\partial\rho}{\partial x} & \frac{\partial\theta}{\partial y} & \frac{\partial\theta}{\partial z} \end{bmatrix} = \begin{bmatrix} \frac{x}{\rho} & \frac{y}{\rho} & \frac{z}{\rho} \\ \frac{-y}{x^2+y^2} & \frac{x}{x^2+y^2} & 0 \\ \frac{-xz}{\rho^2\sqrt{x^2+y^2}} & \frac{-yz}{\rho^2\sqrt{x^2+y^2}} & \frac{1}{z^2} - \frac{1}{\rho^2} \end{bmatrix}, \tag{90}$$

where $\rho = \sqrt{x^2 + y^2 + z^2}$.

$$\mathrm{DCRB}(xy) = \frac{1}{\det}\left(\left(f_{xz} - \frac{2\|\boldsymbol{\alpha}\|^2}{M_T M_R \sigma^2} u_x u_z\right)\left(f_{zy} - \frac{2\|\boldsymbol{\alpha}\|^2}{M_T M_R \sigma^2} u_y u_z\right) - \left(f_{xy} - \frac{2\|\boldsymbol{\alpha}\|^2}{M_T M_R \sigma^2} u_x u_y\right)\left(f_{zz} - \frac{2\|\boldsymbol{\alpha}\|^2}{M_T M_R \sigma^2} u_z^2\right)\right), \tag{83}$$

$$\mathrm{DCRB}(yz) = \frac{1}{\det}\left(\left(f_{xz} - \frac{2\|\boldsymbol{\alpha}\|^2}{M_T M_R \sigma^2} u_x u_z\right)\left(f_{yx} - \frac{2\|\boldsymbol{\alpha}\|^2}{M_T M_R \sigma^2} u_x u_y\right) - \left(f_{yz} - \frac{2\|\boldsymbol{\alpha}\|^2}{M_T M_R \sigma^2} u_y u_z\right)\left(f_{xx} - \frac{2\|\boldsymbol{\alpha}\|^2}{M_T M_R \sigma^2} u_x^2\right)\right), \tag{84}$$

$$\mathrm{DCRB}(xz) = \frac{1}{\det}\left(\left(f_{xy} - \frac{2\|\boldsymbol{\alpha}\|^2}{M_T M_R \sigma^2} u_x u_y\right)\left(f_{yz} - \frac{2\|\boldsymbol{\alpha}\|^2}{M_T M_R \sigma^2} u_y u_z\right) - \left(f_{xz} - \frac{2\|\boldsymbol{\alpha}\|^2}{M_T M_R \sigma^2} u_x u_z\right)\left(f_{yy} - \frac{2\|\boldsymbol{\alpha}\|^2}{M_T M_R \sigma^2} u_y^2\right)\right). \tag{85}$$

REFERENCES

[1] C. Balanis, *Antenna Theory: Analysis and Design*. Wiley, 1996. [Online]. Available: https://books.google.de/books?id=-FsvuAEACAAJ

[2] P. R. Singh, Y. Wang, and P. Chargé, "Bistatic MIMO radar for near field source localisation using PARAFAC," *Electron. Lett.*, vol. 52, no. 12, pp. 1060–1061, 2016.

[3] M. Haardt, R. N. Challa, and S. Shamsunder, "Improved bearing and range estimation via high-order subspace based unitary ESPRIT," in *Proc. 30th Asilomar Conf. Signals, Syst. Comput.*, vol. 1, Nov. 1996, pp. 380–384.

[4] P. R. Singh, Y. Wang, and P. Chargé, "Near field targets localization using bistatic MIMO system with symmetric arrays," in *Proc. 25th Eur. Signal Process. Conf.*, Aug. 2017, pp. 2403–2407.

[5] E. Zhou, H. Jiang, and H. Qi, "4-D parameter estimation in bistatic MIMO radar for near-field target localization," in *Proc. IEEE Int. Wireless Symp.*, Mar. 2015, pp. 1–4.

[6] P. R. Singh, Y. Wang, and P. Charge, "Near field targets localization using bistatic MIMO system with spherical wavefront based model," in *Proc. 25th Eur. Signal Process. Conf.*, Aug. 2017, pp. 2408–2412.

[7] Y. Begriche, M. Thameri, and K. Abed-Meraim, "Exact Cramér-Rao bound for near field source localization," in *Proc. 11th Int. Conf. Inf. Sci., Signal Process. Appl.*, Jul. 2012, pp. 718–721.

[8] I. Podkurkov, L. Hamidullina, E. Traikov, M. Haardt, and A. Nadeev, "Tensor-based near-field localization in bistatic MIMO radar systems," in *Proc. 22nd Int. ITG Workshop Smart Antennas*, Mar. 2018, pp. 1–8.

[9] G. Liu and X. Sun, "Efficient method of passive localization for mixed far-field and near-field sources," *IEEE Antennas Wireless Propag. Lett.*, vol. 12, pp. 902–905, 2013.

[10] R. Schmidt, "Multiple emitter location and signal parameter estimation," *IEEE Trans. Antennas Propag.*, vol. AP-34, no. 3, pp. 276–280, Mar. 1986.

[11] R. Roy and T. Kailath, "ESPRIT-estimation of signal parameters via rotational invariance techniques," *IEEE Trans. Acoust., Speech, Signal Process.*, vol. 37, no. 7, pp. 984–995, Jul. 1989.

[12] L. Kumar and R. M. Hegde, "Near-field acoustic source localization and beamforming in spherical harmonics domain," *IEEE Trans. Signal Process.*, vol. 64, no. 13, pp. 3351–3361, Jul. 2016.

[13] B. Park, H. Lee, P. K. Upputuri, M. Pramanik, D. Kim, and C. Kim, "Super-resolution photoacoustic microscopy using near-field localization by a plasmonic metal nanoaperture: A simulation study," *IEEE J. Sel. Topics Quant. Electron.*, vol. 25, no. 2, pp. 1–7, Mar./Apr. 2019, Art. no. 4600107.

[14] R. Jin and K. Zeng, "Secure inductive-coupled near field communication at physical layer," *IEEE Trans. Inf. Forensics Secur.*, vol. 13, no. 12, pp. 3078–3093, Dec. 2018.

[15] X. Li, X. Ma, and M. Chen, "Bistatic MIMO sonar system based on subarrary and waveform diversity," in *Proc. OCEANS* Aberdeen, 2017, pp. 1–4.

[16] N. Willis and H. Griffiths, *Advances in Bistatic Radar*. Scitech Publishing, 2007. [Online]. Available: https://digital-library.theiet.org/content/books/ra/sbra001e

[17] D. J. Rabideau and P. Parker, "Ubiquitous MIMO multifunction digital array radar," in *Proc. 37th Asilomar Conf. Signals, Syst. Comput.*, 2003, vol. 1, 2003, pp. 1057–1064.

[18] D. R. Fuhrmann and G. S. Antonio, "Transmit beamforming for MIMO radar systems using partial signal correlation," in *Proc. Conf. Rec. 38th Asilomar Conf. Signals, Syst. Comput.*, 2004., vol. 1, 2004, pp. 295–299.

[19] A. M. Haimovich, R. S. Blum, and L. J. Cimini, "MIMO radar with widely separated antennas," *IEEE Signal Process. Mag.*, vol. 25, no. 1, pp. 116–129, 2008.

[20] H. Cramér, *Mathematical Methods of Statistics*. Princeton, NJ, USA: Princeton Univ. Press, 1999.

[21] S. M. Kay, *Fundamentals of Statistical Signal Processing: Estimation Theory*. Englewood Cliffs, NJ, USA: Prentice Hall, 1997.

[22] S. Haykin and K. J. R. Liu, *Handbook on Array Processing and Sensor Networks*. Hoboken, NJ, USA: Wiley, 2009.

[23] A. J. Weiss and B. Friedlander, "Range and bearing estimation using polynomial rooting," *IEEE J. Ocean. Eng.*, vol. 18, no. 2, pp. 130–137, Apr. 1993.

[24] E. Grosicki, K. Abed-Meraim, and Y. Hua, "A weighted linear prediction method for near-field source localization," *IEEE Trans. Signal Process.*, vol. 53, no. 10, pp. 3651–3660, Oct. 2005.

[25] M. N. El Korso, R. Boyer, A. Renaux, and S. Marcos, "Conditional and unconditional Cramér-Rao bounds for near-field source localization," *IEEE Trans. Signal Process.*, vol. 58, no. 5, pp. 2901–2907, May 2010.

[26] Y. Zheng, B. Chen, and M. Yang, "Cramer-Rao bound of the estimation of direction of arrival for low angle targets," in *Proc. CIE Int. Conf. Radar*, 2016, pp. 1–4.

[27] L. Zhang, Q. Huang, and Y. Fang, "Conditional and unconditional CRB of DOA estimation in spherical harmonics domain," in *Proc. IEEE 13th Int. Conf. Signal Process.*, 2016, pp. 424–428.

[28] A. M. Molaei, B. Zakeri, and S. M. H. Andargoli, "Closed-form expression of stochastic CRB for mixed near-field and far-field sources in multipath propagation environments," *IEEE Commun. Lett.*, vol. 23, no. 4, pp. 640–643, Apr. 2019.

[29] R. Gui, W. Wang, C. Cui, and H. C. So, "Coherent Pulsed-FDA radar receiver design with time-variance consideration: SINR and CRB analysis," *IEEE Trans. Signal Process.*, vol. 66, no. 1, pp. 200–214, Jan. 2018.

[30] A. Bazzi and D. Slock, "Cramér-Rao bound for joint angle and delay estimators by partial relaxation," in *Proc. IEEE Global Conf. Signal Inf. Process.*, 2019, pp. 1–5.

[31] H. Cui, W. Peng, T. Liu, and X. Wei, "Cramér-Rao bounds for multiple near field sources location under unknown gain/phase response," in *Proc. 29th Chin. Control Decis. Conf.*, 2017, pp. 5169–5173.

[32] H. Gazzah and J.-P. Delmas, "CRB-Based design of linear antenna arrays for near-field source localization," *IEEE Trans. Antennas Propag.*, vol. 62, no. 4, pp. 1965–1974, Apr. 2014.

[33] T. Bao, M. N. El Korso, and H. H. Ouslimani, "Cramér-Rao bound and statistical resolution limit investigation for near-field source localization," *Digit. Signal Process.*, vol. 48, pp. 137–147, 2016.

[34] S. T. Smith, "Statistical resolution limits and the complexified Cramér-Rao bound," *IEEE Trans. Signal Process.*, vol. 53, no. 5, pp. 1597–1609, May 2005.

[35] Z. Liu and A. Nehorai, "Statistical angular resolution limit for point sources," *IEEE Trans. Signal Process.*, vol. 55, no. 11, pp. 5521–5527, Nov. 2007.

[36] T. Routtenberg and J. Tabrikian, "Non-Bayesian periodic Cramér-Rao bound," *IEEE Trans. Signal Process.*, vol. 61, no. 4, pp. 1019–1032, Feb. 2013.

[37] R. G. McKilliam, B. G. Quinn, and I. V. L. Clarkson, "Direction estimation by minimum squared arc length," *IEEE Trans. Signal Process.*, vol. 60, no. 5, pp. 2115–2124, May 2012.

[38] J. Du *et al.*, "Bistatic MIMO system with uniform circular arc arrays for single near field target localization," in *Proc. 10th Int. Conf. Commun. Softw. Netw.*, 2018, pp. 357–360.

[39] L. De Lathauwer, B. De Moor, and J. Vandewalle, "A multilinear singular value decomposition," *SIAM J. Matrix Anal. Appl.*, vol. 21, no. 4, pp. 1253–1278, 2000.

[40] L. Scharf and C. Demeure, *Statistical Signal Processing: Detection, Estimation, and Time Series Analysis, Ser. Addison-Wesley Series in Electrical and Computer Engineering*. Reading, MA, USA: Addison-Wesley Publishing Company, 1991.

[41] P. Stoica and R. Moses, *Spectral Analysis of Signals*. Englewood Cliffs, NJ, USA: Pearson Prentice Hall, 2005.

[42] E. V. Haynsworth, "On the schur complement," *Basel Math. Notes*, (University of Basel), BMN 20, 1968.

[43] P. Stoica, E. G. Larsson, and A. B. Gershman, "The stochastic CRB for array processing: A textbook derivation," *IEEE Signal Process. Lett.*, vol. 8, no. 5, pp. 148–150, May 2001.

[44] F. Roemer and M. Haardt, "A semi-algebraic framework for approximate CP decompositions via simultaneous matrix diagonalizations (SECSI)," *Signal Process.*, vol. 93, no. 9, pp. 2722–2738, 2013.

[45] R. Bro, N. D. Sidiropoulos, and G. B. Giannakis, "A fast least squares algorithm for separating trilinear mixtures," in *Proc. Int. Workshop Independent Compon. Anal. Blind Signal Separation*, 1999, pp. 11–15.

[46] P. Stoica and A. Nehorai, "Performance study of conditional and unconditional direction-of-arrival estimation," *IEEE Trans. Acoust., Speech, Signal Process.*, vol. 38, no. 10, pp. 1783–1795, Oct. 1990.

Liana Khamidullina (Student Member, IEEE) received the B.E. degree in telecommunications from Kazan National Research Technical University, Kazan, Russia, in 2016 and the M.Sc. degree in communications and signal processing from the German Russian Institute of Advanced Technologies organized between Kazan National Research Technical University, and Ilmenau University of Technology, Ilmenau, Germany, as a double degree program, in 2018. She is currently working toward the Ph.D. degree in communications and signal processing with the Ilmenau University of Technology.

Since 2019, she has been a Research Assistant with Communications Research Laboratory, Ilmenau University of Technology. Her research interests include tensor-based signal processing, multiuser MIMO precoding, radar, direction of arrival estimation, and biomedical signal processing.

Ivan Podkurkov (Student Member, IEEE) received the B.E. degree in telecommunications from Kazan National Research Technical University - KAI (KNRTU-KAI, former Kazan Aviation Institute), Kazan, Russia, in 2014, and the M.Sc. degree in communications and signal processing from the German Russian Institute of Advanced Technologies organized between KNRTU-KAI and TU Ilmenau University of Technology (TUIL), Ilmenau, Germany, as a double degree program, in 2016. He is currently working toward the dual Ph.D. degree with KNRTU-KAI and TUIL. He is curently with the Department of Radio Electronic and Telecommunication Systems, KNRTU-KAI and Communications Research Laboratory, TUIL.

From 2014 to 2016, he was an Engineer, and from 2016 to 2018, a part-time Teaching Assistant with the Department of Radio Electronic and Telecommunication Systems of the Radio Electronic and Telecommunication Institute, KNRTU-KAI. Since October 2016, he has been an Electrical Engineer with ELEPS Ltd., Kazan, Russia.

His research interests include radar, direction of arrival estimation, statistical and tensor-based signal processing, and advanced nongaussian interference models.

Martin Haardt (Fellow, IEEE) studied electrical engineering with Ruhr-University Bochum, Bochum, Germany, and Purdue University, West Lafayette, IN, USA. He received the Diplom-Ingenieur (M.S.) degree from the Ruhr-University Bochum in 1991 and the Doktor-Ingenieur (Ph.D.) degree from Munich University of Technology, Munich, Germany, in 1996. Since 2001, he has been a Full Professor with the Department of Electrical Engineering and Information Technology and the Head of the Communications Research Laboratory, Ilmenau University of Technology, Ilmenau, Germany. His research interests include wireless communications, array signal processing, high-resolution parameter estimation, and tensor-based signal processing.

In 1997, he joined Siemens Mobile Networks, Munich, Germany, where he was responsible for strategic research for third generation mobile radio systems. From 1998 to 2001, he was the Director for International Projects and University Cooperations in the mobile infrastructure business of Siemens in Munich, where his work focused on mobile communications beyond the third generation.

He was the recipient of the 2009 Best Paper Award from the IEEE Signal Processing Society, the Vodafone Innovations Award for outstanding research in mobile communications, the ITG Best Paper Award from the Association of Electrical Engineering, Electronics, and Information Technology, and the Rohde & Schwarz Outstanding Dissertation Award.

He has been or was the Senior Editor of the IEEE JOURNAL OF SELECTED TOPICS IN SIGNAL PROCESSING since 2019, an Associate Editor for the IEEE TRANSACTIONS ON SIGNAL PROCESSING from 2002 to 2006 and from 2011 to 2015, the IEEE SIGNAL PROCESSING LETTERS from 2006 to 2010, the *Research Letters in Signal Processing* from 2007 to 2009, the *Hindawi Journal of Electrical and Computer Engineering* since 2009, the *EURASIP Signal Processing Journal* from 2011 to 2014, and the Guest Editor of the *EURASIP Journal on Wireless Communications and Networking*.

From 2011 until 2019, he was an Elected Member of the Sensor Array and Multichannel technical committee of the IEEE Signal Processing Society, where he was the Vice Chair from 2015 to 2016, Chair from 2017 to 2018, and Past Chair in 2019. Since 2020, he has been an Elected Member of the Signal Processing Theory and Methods (SPTM) Technical Committee of the IEEE Signal Processing Society.

Moreover, he was the Technical Co-Chair of PIMRC 2005 in Berlin, Germany, ISWCS 2010 in York, U.K., the European Wireless 2014 in Barcelona, Spain, and the Asilomar Conference on Signals, Systems, and Computers 2018, USA, and the General Co-chair of WSA 2013 in Stuttgart, Germany, ISWCS 2013 in Ilmenau, Germany, CAMSAP 2013 in Saint Martin, French Antilles, WSA 2015 in Ilmenau, SAM 2016 in Rio de Janeiro, Brazil, CAMSAP 2017 in Curacao, Dutch Antilles, SAM 2020 in Hangzhou, China, and the Asilomar Conference on Signals, Systems, and Computers 2021, USA.